NASA TN D-1648

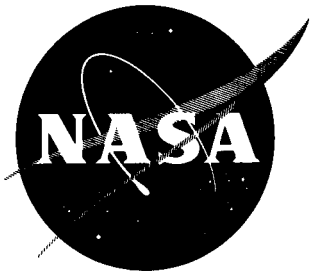

TECHNICAL NOTE

D-1648

STATIC AERODYNAMIC CHARACTERISTICS OF A SHORT BLUNT 10° SEMIVERTEX ANGLE CONE AT A MACH NUMBER OF 15 IN HELIUM

By Melvin J. Fohrman

Ames Research Center
Moffett Field, Calif.

NATIONAL AERONAUTICS AND SPACE ADMINISTRATION
WASHINGTON

February 1963

NATIONAL AERONAUTICS AND SPACE ADMINISTRATION

TECHNICAL NOTE D-1648

STATIC AERODYNAMIC CHARACTERISTICS OF A SHORT BLUNT 10° SEMIVERTEX ANGLE CONE AT A MACH NUMBER OF 15 IN HELIUM

By Melvin J. Fohrman

SUMMARY

Axial force, normal force, pitching moment, and shock-wave shape were determined for a body of revolution consisting of a short blunt 10° semivertex angle cone with a flat base and also with a conical afterbody having a semivertex angle of 50°. Measurements were made in helium at a free-stream Mach number of 15 and a free-stream Reynolds number of 2.25×10^6 based on maximum body diameter over an angle-of-attack range from 0° to 180°.

The configuration with the conical afterbody was statically stable in the nose-forward attitude only, whereas the configuration with no afterbody was statically stable in both the nose-forward and base-forward attitudes. The force and moment data of both shapes were predicted reasonably well by modified Newtonian theory at all angles of attack, except the pitching-moment coefficient for the model without afterbody near 180° angle of attack. In this region, measurements indicated static stability, whereas theory indicated static instability. The helium data agreed reasonably well with a limited amount of force and moment data obtained in a ballistic range at small angles of attack in air at a Mach number of 15 and also with force and moment data obtained in air over a complete angle-of-attack range at a Mach number of 5.5. The value of axial-force coefficient and the shape of the bow shock wave at zero angle of attack for both models obtained from a numerical flow field calculation agreed very well with the data. The value of the axial force coefficient at 180° angle of attack for the model with afterbody agreed reasonably well with the theoretical value for a cone. The position and shape of the shock envelope near the stagnation point also could be predicted accurately by an approximate method over an angle-of-attack range from 0° to 60°.

INTRODUCTION

Aerodynamic data on various vehicle shapes is needed for designing unmanned instrumented probe vehicles for exploring the atmospheres of near-Earth planets. An aerodynamic requirement for such a vehicle may be that it be statically stable in only one attitude. The reason for imposing this requirement is that

aerodynamic effects would orient the vehicle properly before it encountered the high-heating-rate portion of the trajectory even though the vehicle began its entry in a random attitude.

A configuration known to satisfy many requirements of an atmospheric probe consists of a blunt-nosed 10° half-angle cone with a flat base. Previous tests, however, have shown that flat-based bodies of revolution are generally statically stable about two trim attitudes, nose forward and base forward. From theoretical considerations it was determined that adding a 50° half-angle conical afterbody to this configuration would eliminate the base-forward stable trim attitude so that unique nose-forward stability would be insured. To investigate the aerodynamic suitability of these two shapes, one having a flat base and the other a conical afterbody, a coordinated study was undertaken at the Ames Research Center. Results from previously completed phases of the experimental portion of this coordinated program, which covered a Mach number range from 0.6 to 15 in air, are presented in references 1 through 4. These results were used in an analysis of the motions of the vehicles during entry into a model Martian atmosphere. (See ref. 5.)

The purpose of the present investigation was twofold: first, to measure the static force and moment characteristics and the shape of the bow shock wave on both vehicles at a high Mach number in the helium tunnel; second, to compare these results with theoretical estimates and experimental wind-tunnel data obtained in air over a limited angle-of-attack range at a high Mach number and over the complete angle-of-attack range at a lower Mach number.

SYMBOLS

A frontal area, $\frac{\pi d^2}{4}$, sq in.

C_A axial-force coefficient, $\frac{\text{axial force}}{qA}$

C_D drag coefficient, $\frac{\text{drag force}}{qA}$

C_m pitching-moment coefficient, $\frac{\text{pitching moment}}{qAd}$

C_N normal-force coefficient, $\frac{\text{normal force}}{qA}$

d maximum body diameter, in.

i_r angle between sting-support axis and longitudinal model axis, deg (see fig. 1(b))

M free-stream Mach number

q free-stream dynamic pressure, psia

Re free-stream Reynolds number based on diameter, d

R_b radius of spherical sector used to approximate model forebody for purpose of analysis, in. (see fig. 10(a))

x, r body fixed cylindrical coordinates (see fig. 10(a))

α angle of attack, referred to body center line, deg

TEST APPARATUS

The tests were conducted in the Ames hypersonic helium tunnel, which is a variable pressure, constant temperature, closed circuit, blowdown tunnel with interchangeable nozzles contoured to obtain Mach numbers of 8, 15, 20, and 26. The tunnel consists of: (1) a high-pressure reservoir for helium storage at 6,000 psia, (2) a heater filled with cast iron pebbles to maintain a constant stagnation temperature during test runs, (3) a 20-inch diameter cylindrical test section (with a boundary layer approximately 5 inches thick leaving a usable test core diameter of about 10 inches) equipped with interchangeable curved or flat optical glass windows for flow visualization, (4) a model support which consists of a position feedback system actuated by hydraulic power and controlled by an electric programmer through an angle-of-attack range from $+30^\circ$ to -15°, (5) a constant diameter diffuser, (6) two spheres for low pressure storage with a total volume of 447,000 cubic feet, (7) a seven stage reciprocating type helium compressor, and (8) a helium purifier which maintains helium at a purity of 99.4 to 99.5 percent by volume during tunnel operation.

The static forces and moments were measured with a five component flexure type strain-gage balance. The balance also served as a support sting for the models. The data were recorded on a Beckman 210 high speed data recording system which converted the analog input into digital information which was stored on magnetic tape.

The two models tested had identical blunt forebodies consisting of a spherical sector tangent to a segment of a torus which was tangent to a frustum of a 10° semivertex angle cone. The models differed in that one had a flat base, whereas the other had an afterbody consisting of a 50° semivertex angle cone. Four sting-mounting arrangements were employed to cover an angle-of-attack range from 0° to 180° for each configuration. Details of the models and sting-support arrangements are shown in figure 1.

TEST PROCEDURE

The tests were conducted at a free-stream Mach number of 15, free-stream Reynolds number of 2.25×10^6 (based on maximum body diameter), a stagnation pressure of 1200 psia, and a stagnation temperature of 70° F. A retractable spike was centered in front of the model before a run in order to reduce the blockage in the test section and thereby enable the tunnel to start. After

steady-state conditions were established, the spike was raised to the upper surface of the test section. The spike was lowered again just before shutdown to reduce the loading on the model during this phase of the run. Axial force, normal force, and pitching moment were measured and shadowgraphs were taken at angles of attack from 0° to 180° in 5° increments. The angle range of data obtained using the various sting-mounting arrangements overlapped in most cases. Good agreement of the overlapping data indicates that the effects of sting interference were small.

On both models the reference moment center used for the data reduction was located 0.482d aft of the nose. (See fig. 1(a).) The base pressure was measured on the model with the flat afterbody at zero angle of attack and was found to be less than the free-stream static pressure so that the base pressures were negligible in comparison to the forebody pressures. The results from the experimental investigation of reference 6 indicate that the Mach number can be considered constant within the test core of the test section and that the stream angle in the test section had a negligible effect on the force and moment coefficients. The effects of compression of the helium in the stagnation chamber (real gas effects) were determined from tabulated thermodynamic properties of helium using the method given in reference 7. Deviations from the ideal gas case amounted to about 2 to 3 percent. The effects of impurities in the helium were estimated to cause about a 1-percent error in the static pressures (used for the determination of Mach number) based on results obtained from experiments performed in reference 8. The errors due to impurities were neglected in the present investigation.

RESULTS AND DISCUSSION

Force and Moment Coefficients

Axial-force, normal-force, and pitching-moment coefficients for angles of attack ranging from 0° to 180° are presented in figure 2 for the model without an afterbody and in figure 3 for the model with an afterbody. Several theories were employed for estimating the aerodynamic characteristics of the models. Variations of all coefficients with angle of attack were estimated by means of Newtonian theory equations of reference 9 modified for the pressure loss through a normal shock. In this method it is assumed that the pressure coefficient is zero (the measured static pressure is equal to the free-stream static pressure) on all parts of the body not facing the free stream. A second method was used to calculate axial-force coefficients for both models at zero angle of attack; the flow field behind the shock wave was calculated using the method of reference 10 which involves a combination of the inverse solution of the blunt-body problem in the subsonic and transonic regions and the method-of-characteristics solution in the supersonic region, but assumes the pressure on the afterbody is zero. At a free-stream Mach number of 15, the free-stream static pressure was essentially zero. The theoretical values for cones presented in reference 11 (herein designated as cone theory) were used to calculate the axial-force coefficient of the model with afterbody at an angle of attack of 180°. All of the theoretical estimates are compared with the experimental data in figures 2 and 3.

For the model without an afterbody, modified Newtonian theory predicts the axial-force and normal-force coefficients very well up to 60° angle of attack and

reasonably well throughout the rest of the angle-of-attack range (figs. 2(a) and 2(b)). Predictions for the pitching-moment coefficients are reasonably good up to angles of attack of 80° (fig. 2(c)). The most significant differences between the modified Newtonian theory and experiment for the pitching-moment coefficients occur at angles of attack near 180° where the theory predicts static instability while the experimental data indicate that the shape is statically stable in the base-forward attitude. This result is consistent with that found in another investigation of this shape at lower Mach numbers in air (ref. 1). The fact that the theory does not adequately predict the stability of this shape at 180° angle of attack may be due to a pressure relieving effect near the edges of the flat base in the actual situation, whereas Newtonian theory predicts a constant pressure over the entire base at a given angle of attack. The axial-force coefficient at zero angle of attack calculated by the numerical flow field analysis (fig. 2(a)) is nearly identical with the experimental data.

For the model with afterbody, the results are shown in figure 3. These results are almost identical to those for the model without afterbody up to angles of attack of about 60°. Above this angle the coefficients are altered somewhat by the presence of the afterbody. The axial-force (except near 180° angle of attack) and normal-force coefficients agree reasonably well with the modified Newtonian theory throughout the angle-of-attack range (see figs. 3(a) and 3(b)). The prediction of the axial-force coefficient at 180° angle of attack based on the theoretical value for cones is considerably different from the Newtonian estimate, the cone theory underestimating and the Newtonian theory overestimating the experimentally determined values. A shadowgraph taken with the model at 180° angle of attack is shown in figure 4. This shadowgraph indicates that the shock wave begins to curve toward the body about halfway along the conical face. Thus, the lack of agreement between the cone theory and experiment may be attributed to the apparent absence of truly conical flow as indicated by this curved shock wave.

The most significant effect of adding the afterbody is the alteration of the pitching-moment curve at large angles of attack. It is shown in figure 3(c) that the model with afterbody is unstable in the base-forward attitude and, furthermore, that Newtonian theory predicts this result. As pointed out in reference 1, this result indicates the configuration without afterbody would probably be a less desirable entry capsule than the configuration with afterbody because its static stability in both the nose-forward and base-forward attitudes would not allow a unique nose-forward attitude to be attained, by aerodynamic effects alone. Therefore thermal protection would be required on both ends of this vehicle.

Comparison of Helium Data With Air Data

To determine whether the helium tunnel results agree with those obtained in air the drag-force and pitching-moment coefficient data of this investigation are compared with air data obtained for the same Mach number in the free-flight tests reported in reference 4. These comparisons for the model without afterbody are shown in figure 5 wherein estimates based on the modified Newtonian theory for air (which includes real gas effects) and helium are also included. The

measured drag coefficients in helium for Re = 2.25×10^6 (see fig. 5(a)) are about 8 percent lower than those obtained in air for Re = 2.8×10^6 for the angle-of-attack range from 0° to 25°. It should be noted that the free-flight testing technique used to obtain the results of reference 4 does not allow an exact measurement of the drag coefficient at a fixed angle of attack, but instead provides an average value of the drag coefficient over complete cycles of oscillatory motion of various amplitudes. The theory provides good estimates of the trends with angle of attack and differences due to gas composition but predicts values about 4 percent high in each case.

The pitching-moment coefficients for helium and air are compared in figure 5(b). The results from the free-flight tests were obtained by a method described in reference 4 which relates the pitching and yawing motions of a symmetrical body in free flight to a cubic variation of pitching moment with angle of attack. Good agreement between the helium and air data is noted for low angles of attack. (This comparison is not entirely conclusive, however, since the techniques used to obtain the air data were quite different from those used to obtain the helium data.) The Newtonian theory indicates that little difference is to be expected between the air and helium data and this is in fact the result that is obtained from a comparison of the data in figure 5(b).

It is also of interest to compare the Mach number 15 helium results of this investigation with the Mach number 5.5 air data of reference 1. The comparison is made in figure 6 for the model without afterbody, and in figure 7 for the model with afterbody for an angle-of-attack range extending from 0° to 180°. Axial-force, normal-force, and pitching-moment coefficients are shown together with estimates based on modified Newtonian theory and cone theory. Excellent agreement in the force and moment characteristics between the two sets of data is noted for both models even though the air data were obtained at a substantially lower Reynolds number. Both modified Newtonian and cone theory provide reasonable estimates of the small differences in the data due to Mach number and gas composition. At 180° angle of attack the cone theory for air also underestimates the experimentally determined level for the air data by about the same amount as the cone theory for helium does for the helium data (see fig. 7(a)). It was observed that the shadowgraphs in reference 1 for the model with afterbody at 180° angle of attack showed the same features that were noted in the present investigation; namely, that the shock wave was attached and that it curved slightly toward the body. Further comparisons of the helium data of this investigation and air data at Mach numbers from 0.6 to 5.5 are made in reference 5 wherein all of the data obtained in the coordinated Ames program for both the models with and without an afterbody are summarized.

Shock-Wave Shapes

An accurate knowledge of the location of the shock wave about the forebody portion of the model is useful for predicting surface pressures and for calculating radiative heat transfer. A typical shadowgraph of the model without afterbody taken at zero angle of attack is shown in figure 8. The shock-wave shape, corrected for magnification errors caused by the curved windows in the wind tunnel is shown in figure 9. The correction is based on an experimental calibration of

the window and is accurate to within 1 percent of the true shock-wave shape. A numerical solution based on reference 8 is also shown in this figure and it is noted that its agreement with the helium data is very good.

A method for defining the shock-wave shape around the forebody portion of bodies with spherical noses at angle of attack is presented in reference 12. This method is based on: (1) the continuity of mass flow between the shock wave and the body surface, (2) oblique shock relationships, and (3) a correlation of stagnation-point velocity gradient with Mach number. In order to apply this method to the present configurations, it was necessary to approximate the forebody of the models with a spherical sector. It was found that a 70° half angle spherical sector with radius equal to 0.442d provided a good approximation to the actual forebody. The trace of the sonic point at the surface was assumed to be located at a polar angle of 45° with respect to the stagnation streamline. The results of the prediction are compared with the data in figure 10. The prediction is valid either in the region where the flow is subsonic or in the subsonic region up to a polar angle of 70° on the body, whichever is smaller. The angle of 70° is the limit to which the hypothetical spherical body approximates the actual one (see fig. 10(d)). The calculations at all angles of attack are based on sonic points located 45° from the stagnation point on the hypothetical spherical body. Therefore the shock-wave shape and stand-off distance about the body stagnation point at all angles of attack are identical. The data agree with the predictions of the shock-wave shape for angles of attack from 0° to 60°. However, at 70° and 80° angle of attack the prediction of the shock position is inaccurate (see figs. 10(h) and 10(i)) probably because of the deviation of the hypothetical body from the actual body. These comparisons indicate that the location of the portion of the shock wave in the vicinity of the stagnation streamline can be predicted reasonably well up to high angles of attack.

SUMMARY OF RESULTS

Force and moment coefficients and shock-wave shapes were measured in helium at $M = 15$ and at $Re = 2.25 \times 10^6$ on two configurations consisting of a short, blunt, 10° semivertex angle conical forebody with no afterbody and with a conical afterbody having a semivertex angle of 50°. Measurements were taken over an angle-of-attack range from 0° to 180°. The following results were obtained:

1. The data indicate that the configuration with a conical afterbody is statically stable in the nose-forward attitude only, whereas the configuration with no afterbody is statically stable in both the nose-forward and base-forward attitudes.

2. The predictions of modified Newtonian theory agree fairly well with the data for axial force, normal force, and pitching moment. The only serious deviation occurs for angles of attack near 180° for the model with no afterbody. In this region, the theory indicates static instability whereas the experiment indicates static stability. The value of the axial-force coefficient obtained from a numerical calculation of the flow field at zero angle of attack agrees quite well with the helium data.

3. The helium data agree reasonably well with the drag and pitching-moment coefficients obtained in air at $M = 15$ and $Re = 2.8 \times 10^6$ (angle-of-attack measurement range from 0° to 25°) and with the axial-force, normal-force, and pitching-moment coefficients in air at $M = 5.5$ and $Re = 0.6 \times 10^6$ (angle-of-attack measurement range from 0° to 180°).

4. The shock-wave shapes obtained from shadowgraphs in the current tests agree well as to the location and shape with a numerical calculation of the flow field at zero angle of attack and with an approximate prediction (applicable to a small region near the stagnation point) over an angle-of-attack range from 0° to 60°.

Ames Research Center
National Aeronautics and Space Administration
Moffett Field, Calif., Nov. 6, 1962

REFERENCES

1. Treon, Stuart L.: Static Aerodynamic Characteristics of Short Blunt Cones With Various Nose and Base Cone Angles at Mach Numbers of 0.6 to 5.5 and Angles of Attack to 180°. NASA TN D-1327, 1962.

2. Intrieri, Peter F.: Free-Flight Measurements of the Static and Dynamic Stability and Drag of a 10° Blunted Cone at Mach Numbers 3.5 and 8.5. NASA TN D-1299, 1962.

3. Wehrend, William R.: Wind-Tunnel Investigation of the Static and Dynamic Stability Characteristics of a 10° Semivertex Angle Blunted Cone. NASA TN D-1202, 1962.

4. Compton, Dale L.: Free-Flight Measurements of Drag and Static Stability for a Blunt-Nosed 10° Half-Angle Cone at Mach Number 15. NASA TM X-507, 1961.

5. Peterson, Victor L.: Motions of a Short 10° Blunted Cone Entering a Martian Atmosphere at Arbitrary Angles of Attack and Arbitrary Pitching Rates. NASA TN D-1326, 1962.

6. Tendeland, Thorval, and Pearson, Byrd D.: Effectiveness of Two Flap Controls on a Mercury Type Capsule at a Mach Number of 15 in the Ames Hypersonic Helium Tunnel. NASA TM X-660, 1962.

7. Erickson, Wayne D.: Real-Gas Correction Factors for Hypersonic Flow Parameters in Helium. NASA TN D-462, 1960.

8. Henderson, Arthur, Jr., and Swalley, Frank E.: Effects of Air Contamination in a Helium Tunnel. NASA TN D-406, 1960.

9. Margolis, Kenneth: Theoretical Evaluation of the Pressures, Forces, and Moments at Hypersonic Speeds Acting on Arbitrary Bodies of Revolution Undergoing Separate and Combined Angle-of-Attack and Pitching Motions. NASA TN D-652, 1961.

10. Inouye, Mamoru, and Lomax, Harvard: Comparison of Experimental and Numerical Results for the Flow of a Perfect Gas About Blunt-Nosed Bodies. NASA TN D-1426, 1962.

11. Mueller, James N.: Equations, Tables, and Figures for Use in the Analysis of Helium Flow at Supersonic and Hypersonic Speeds. NASA TN D-4063, 1957.

12. Kaattari, George E.: Predicted Shock Envelopes about Two Types of Vehicles at Large Angles of Attack. NASA TN D-860, 1961.

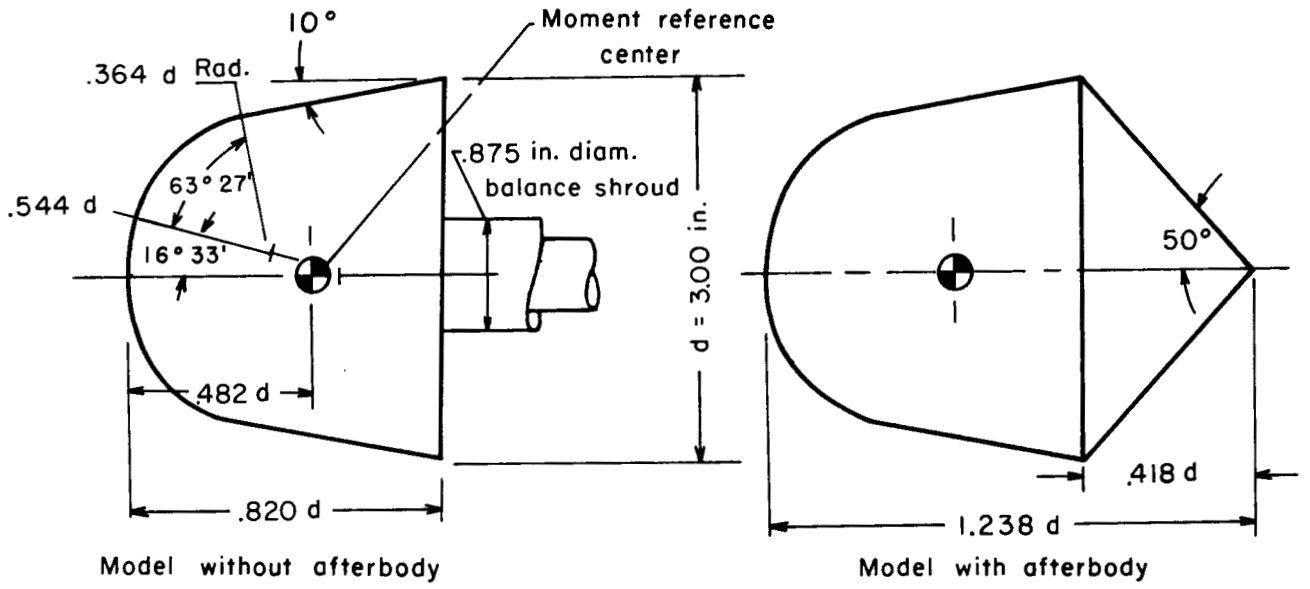

(a) Model details.

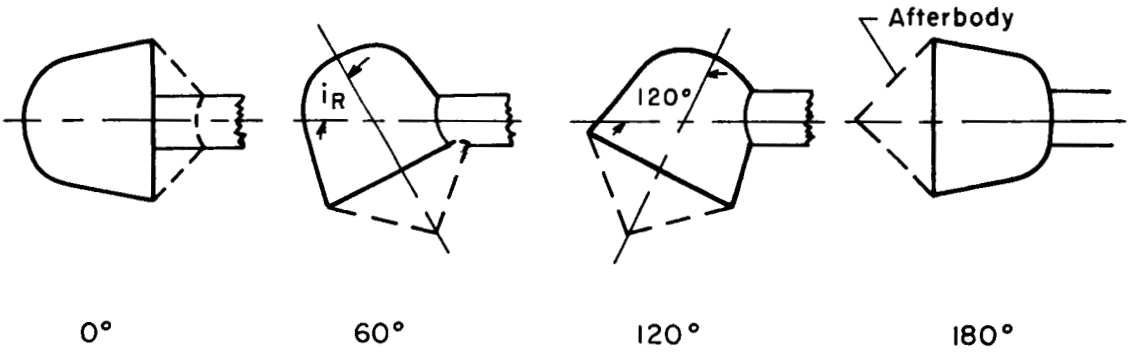

(b) Support arrangement for model.

Figure 1.- Models and their support arrangements.

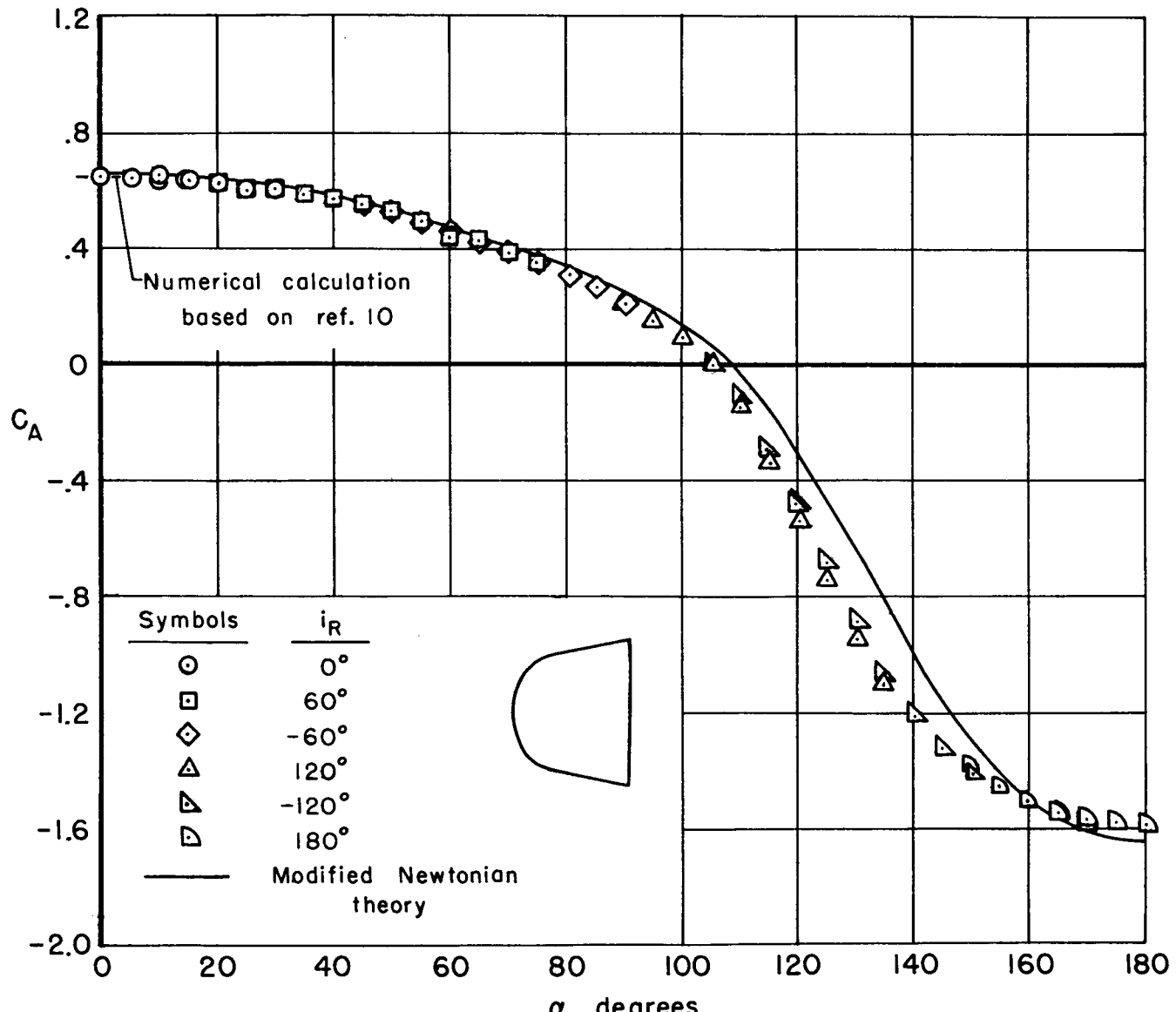

(a) C_A vs. α

Figure 2.- Static aerodynamic coefficients of model without afterbody at M = 15 in helium.

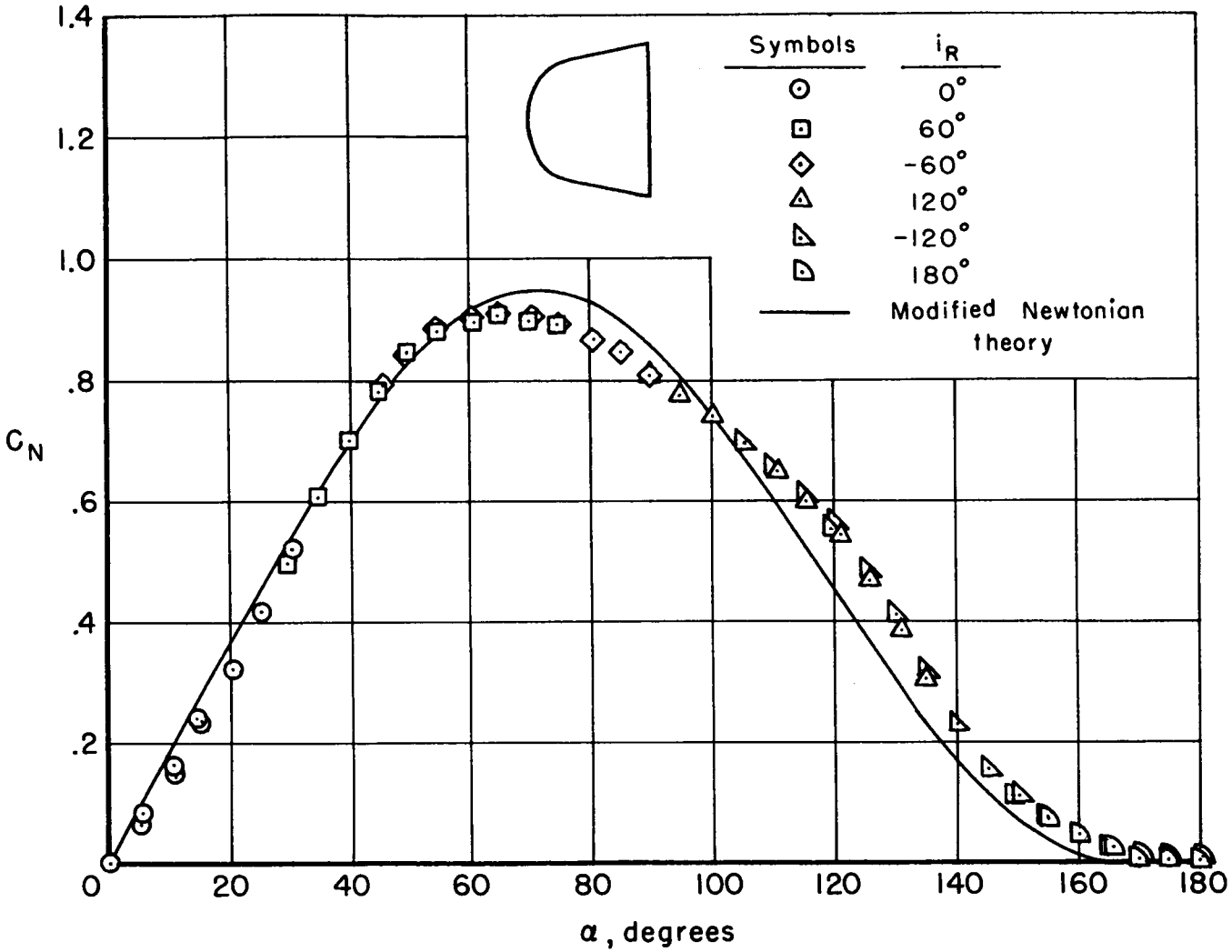

(b) C_N vs. α

Figure 2.- Continued.

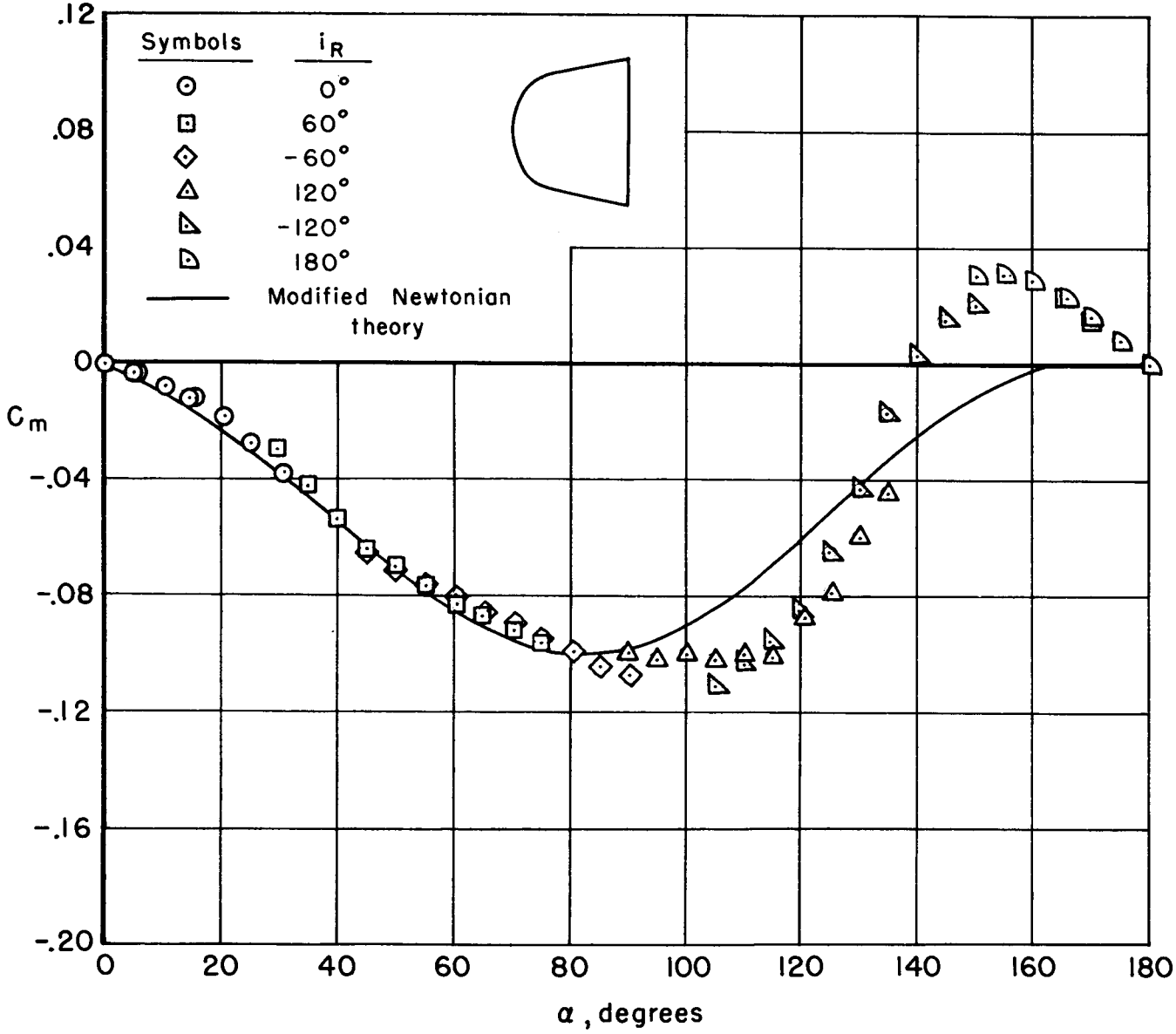

(c) C_m vs. α

Figure 2.- Concluded.

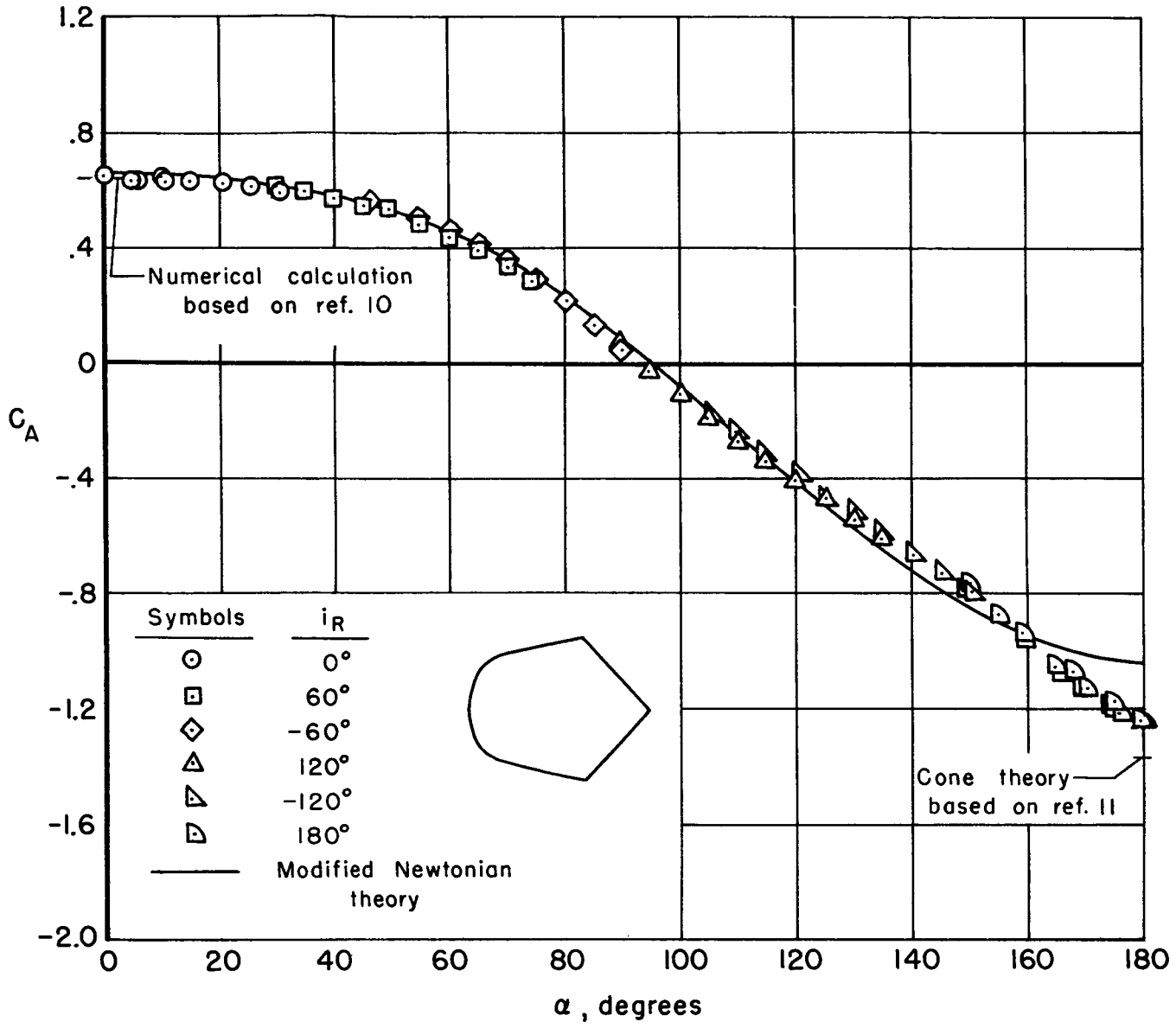

(a) C_A vs. α

Figure 3.- Static aerodynamic coefficients of model without afterbody at M = 15 in helium.

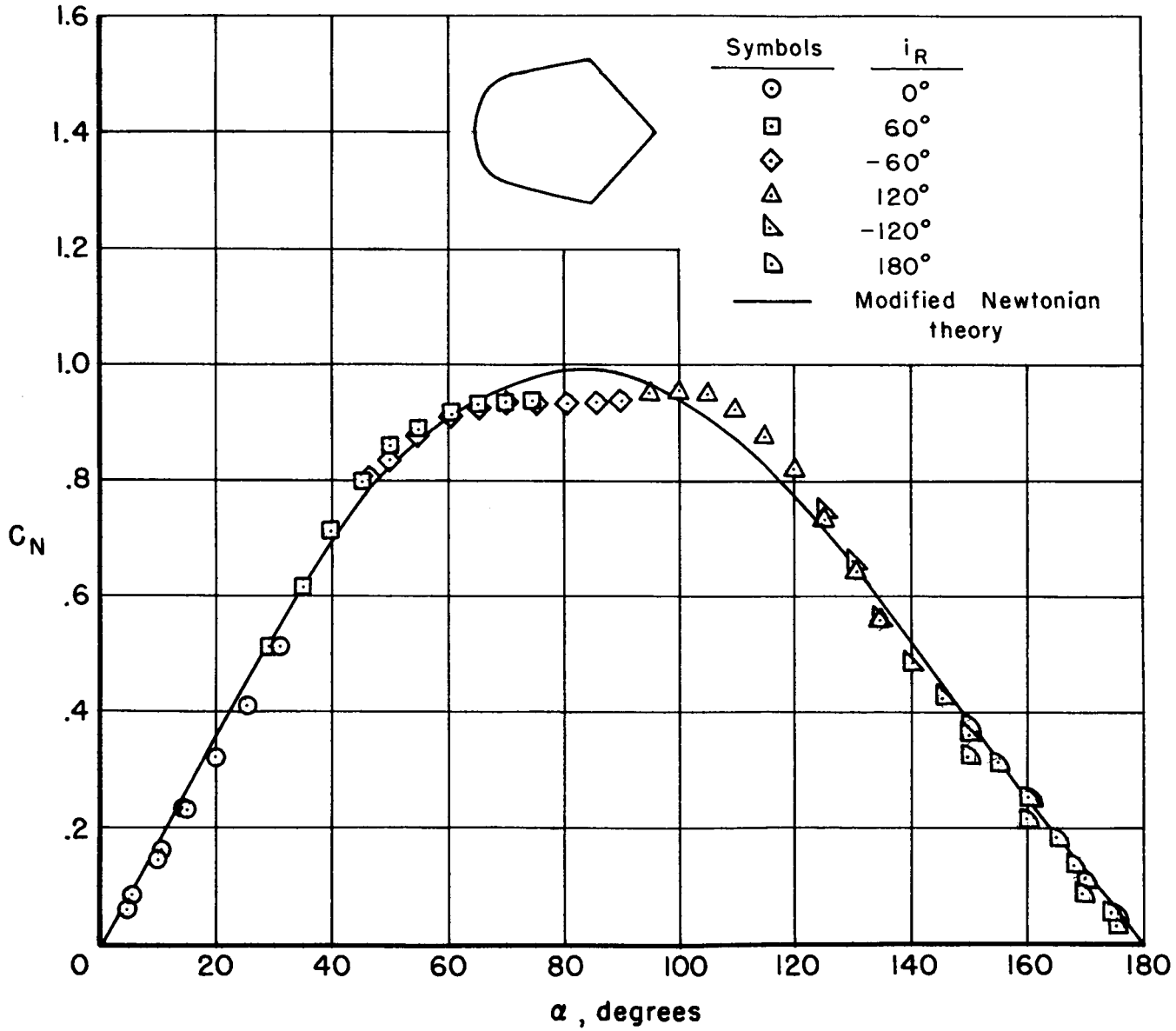

(b) C_N vs. α

Figure 3.- Continued.

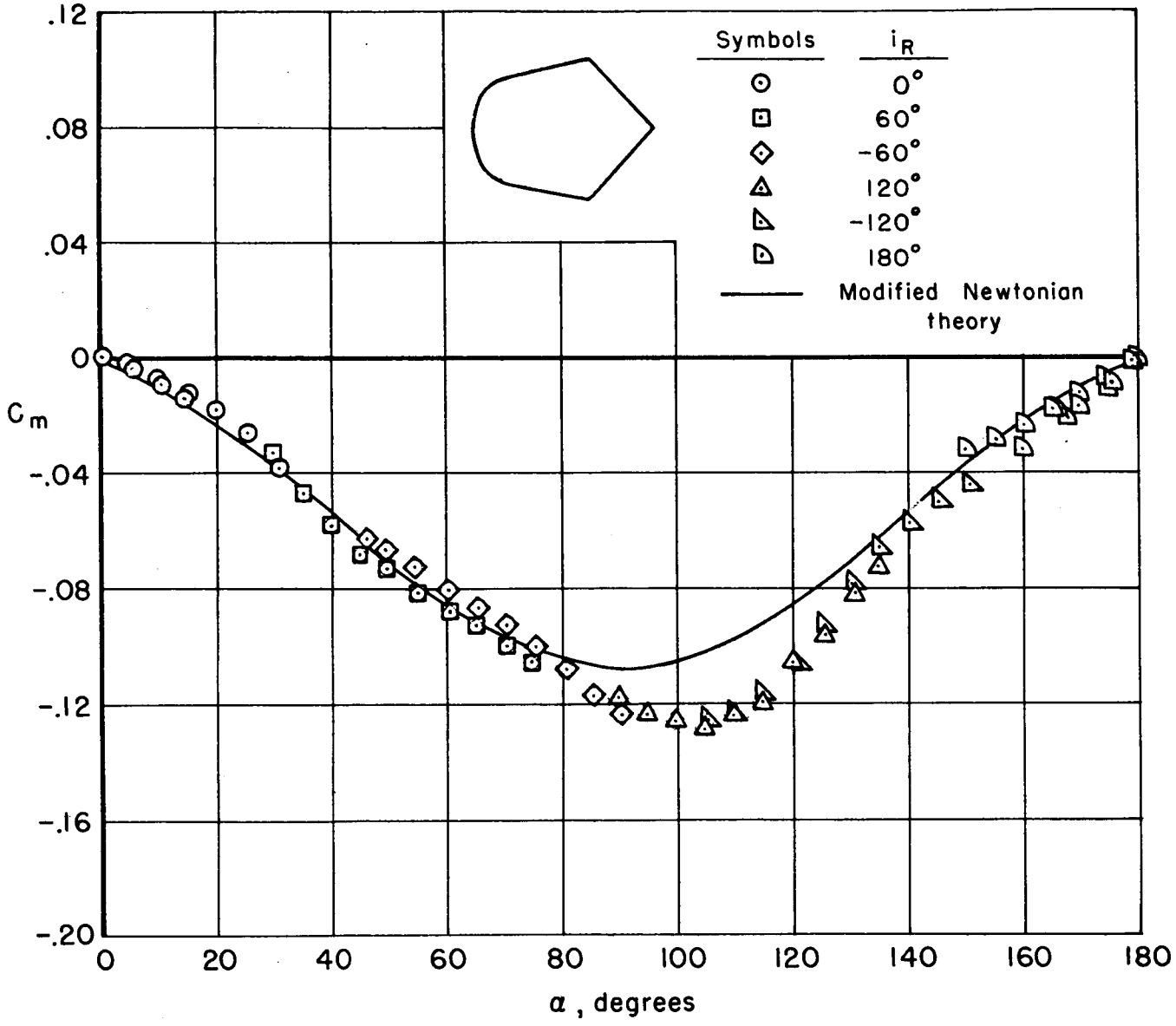

(c) C_m vs. α

Figure 3.- Concluded.

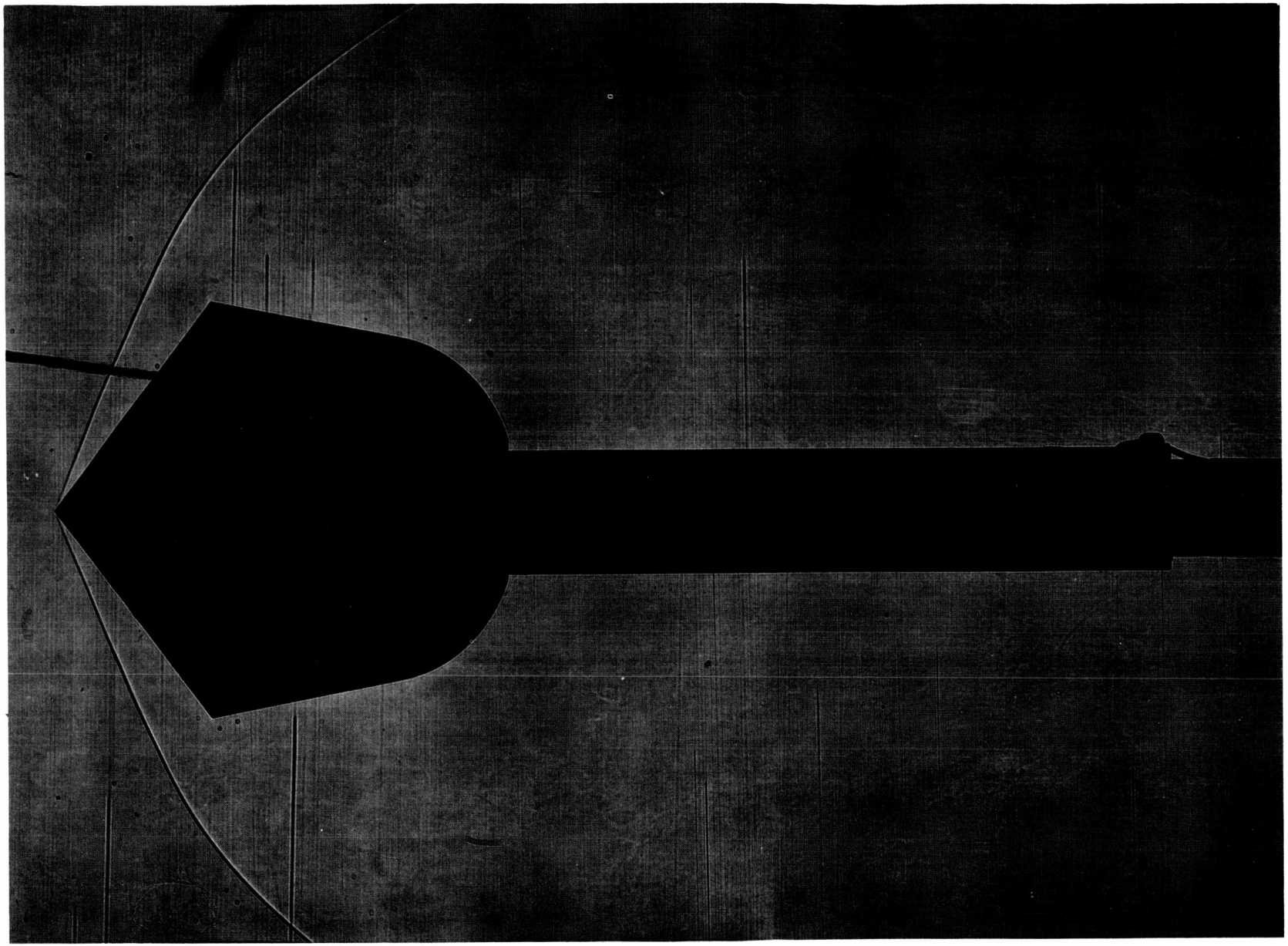

Figure 4.- Shadowgraph of model with afterbody in M = 15 helium flow, $\alpha = 180^{\circ}$.

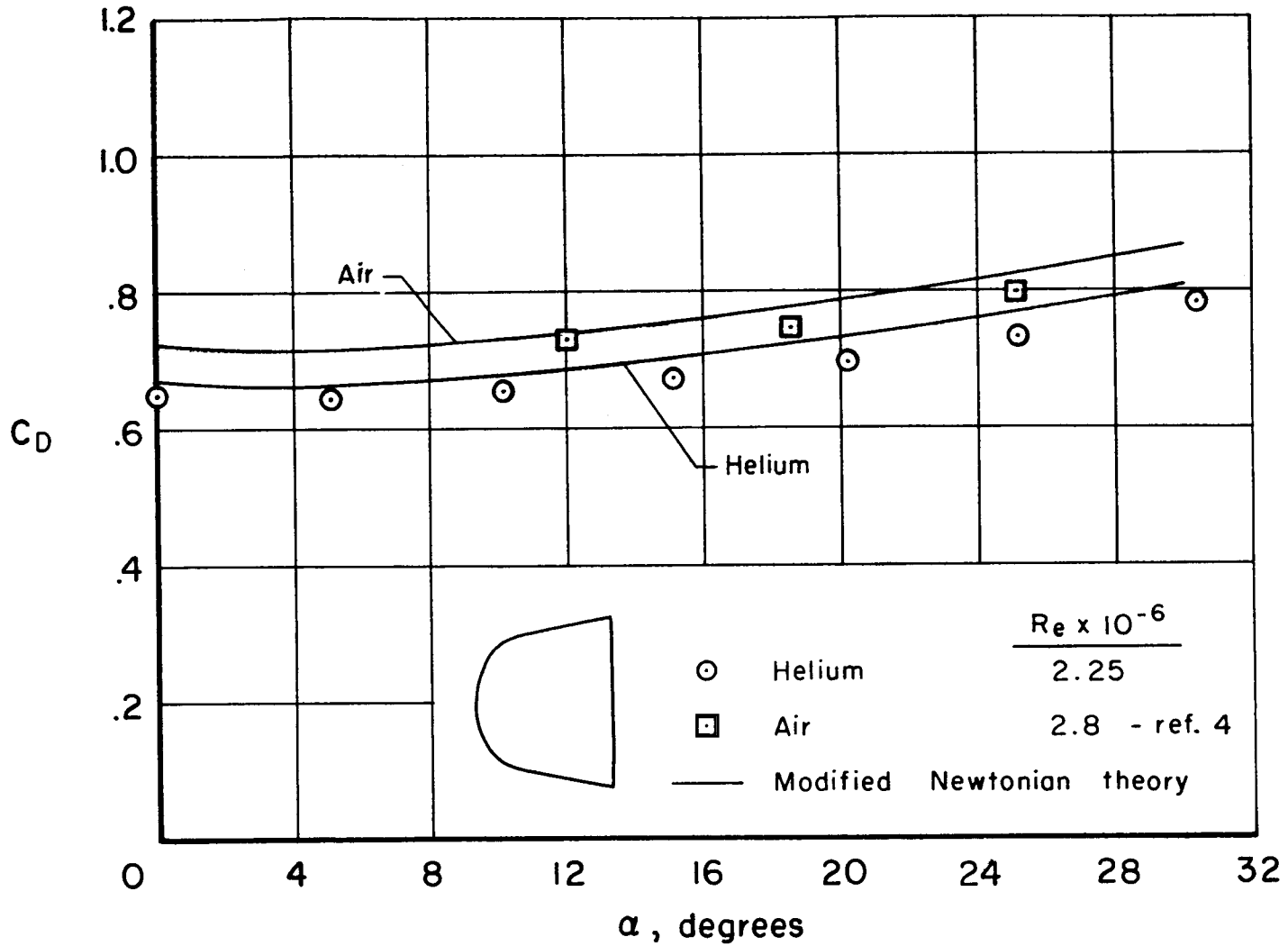

(a) C_D vs. α

Figure 5.- Comparison of static aerodynamic coefficients of model without afterbody at M = 15 in helium and air.

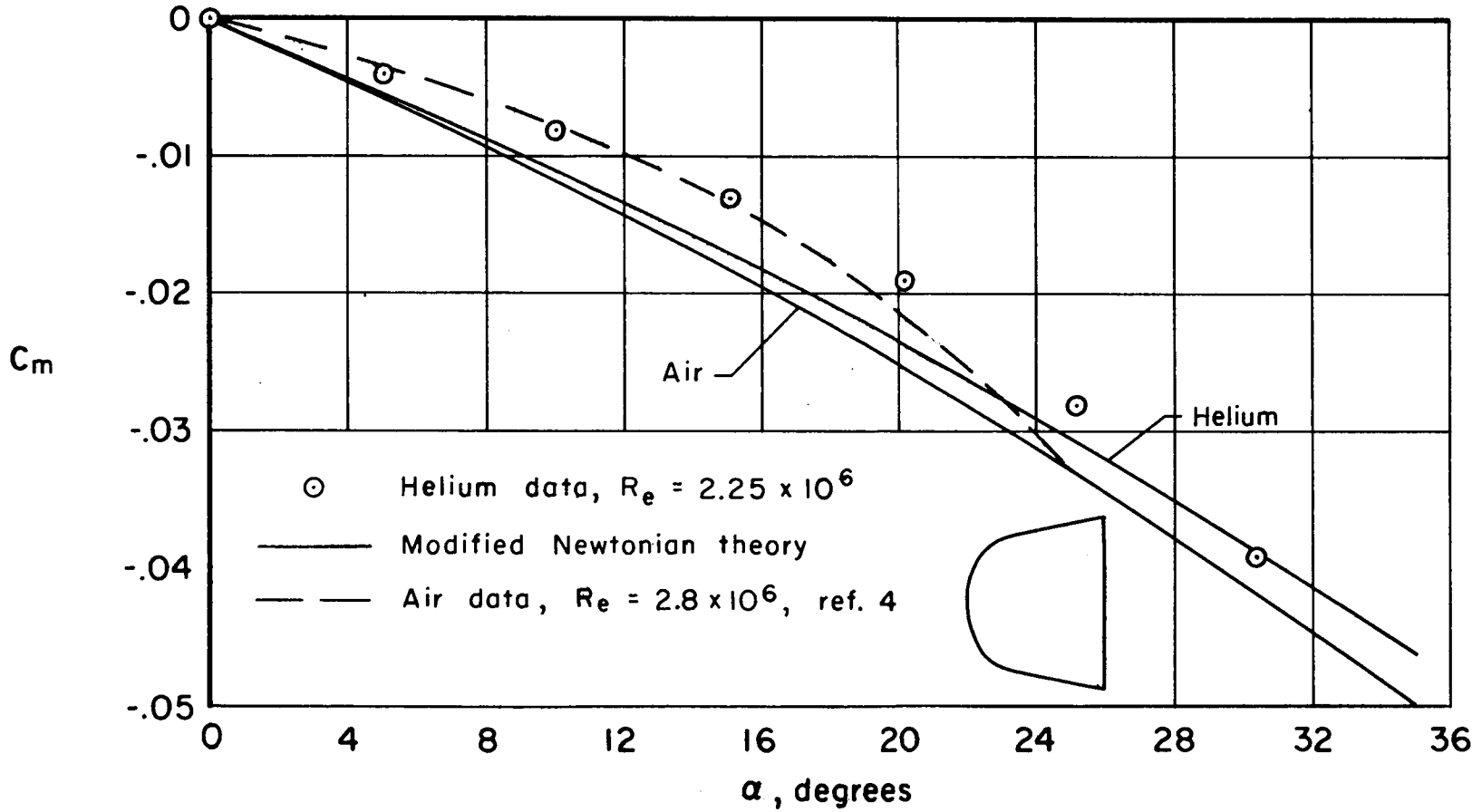

(b) C_m vs. α

Figure 5.- Concluded.

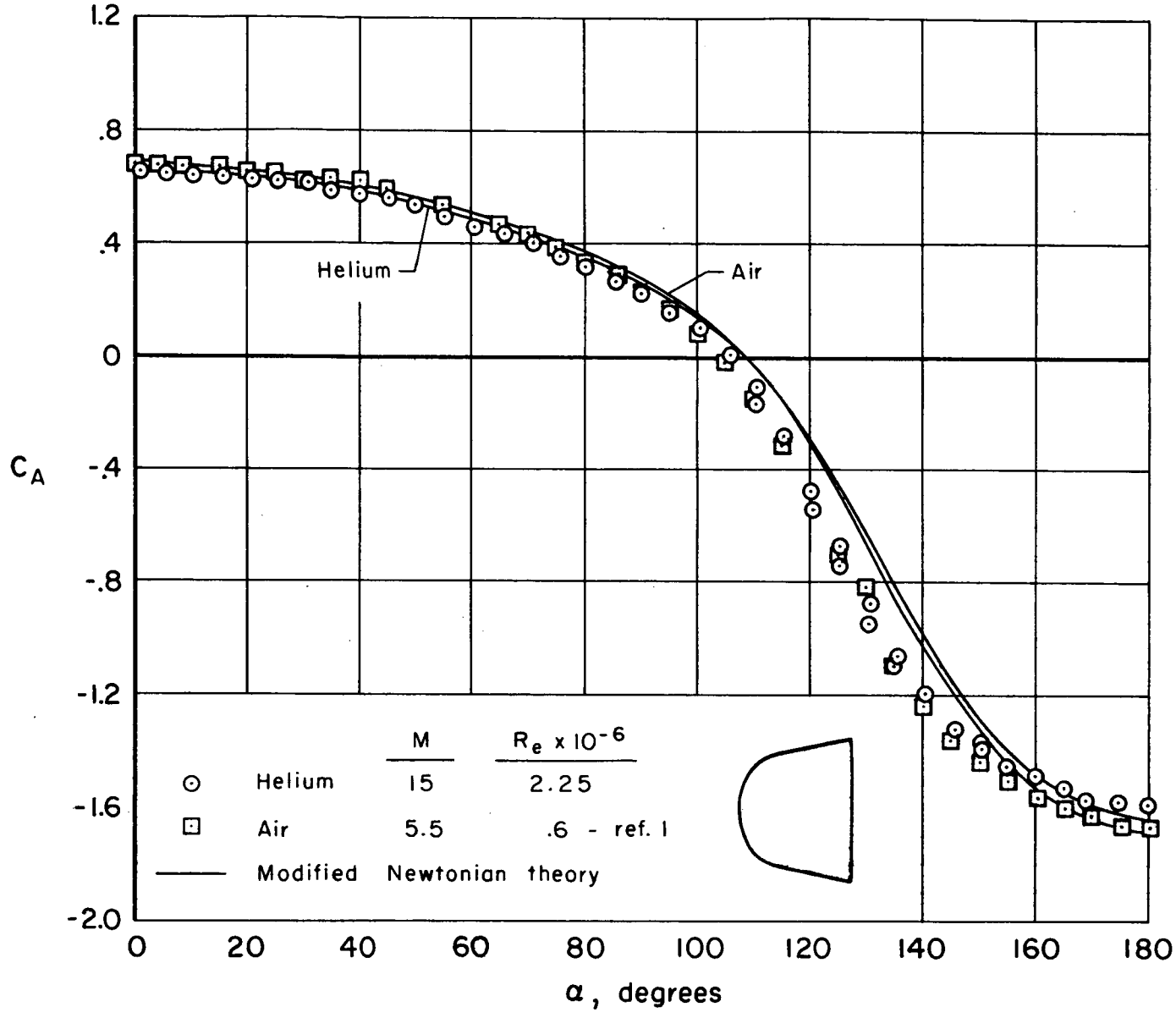

(a) C_A vs. α

Figure 6.- Comparison of static aerodynamic coefficients for model without afterbody at M = 15 in helium and M = 5.5 in air.

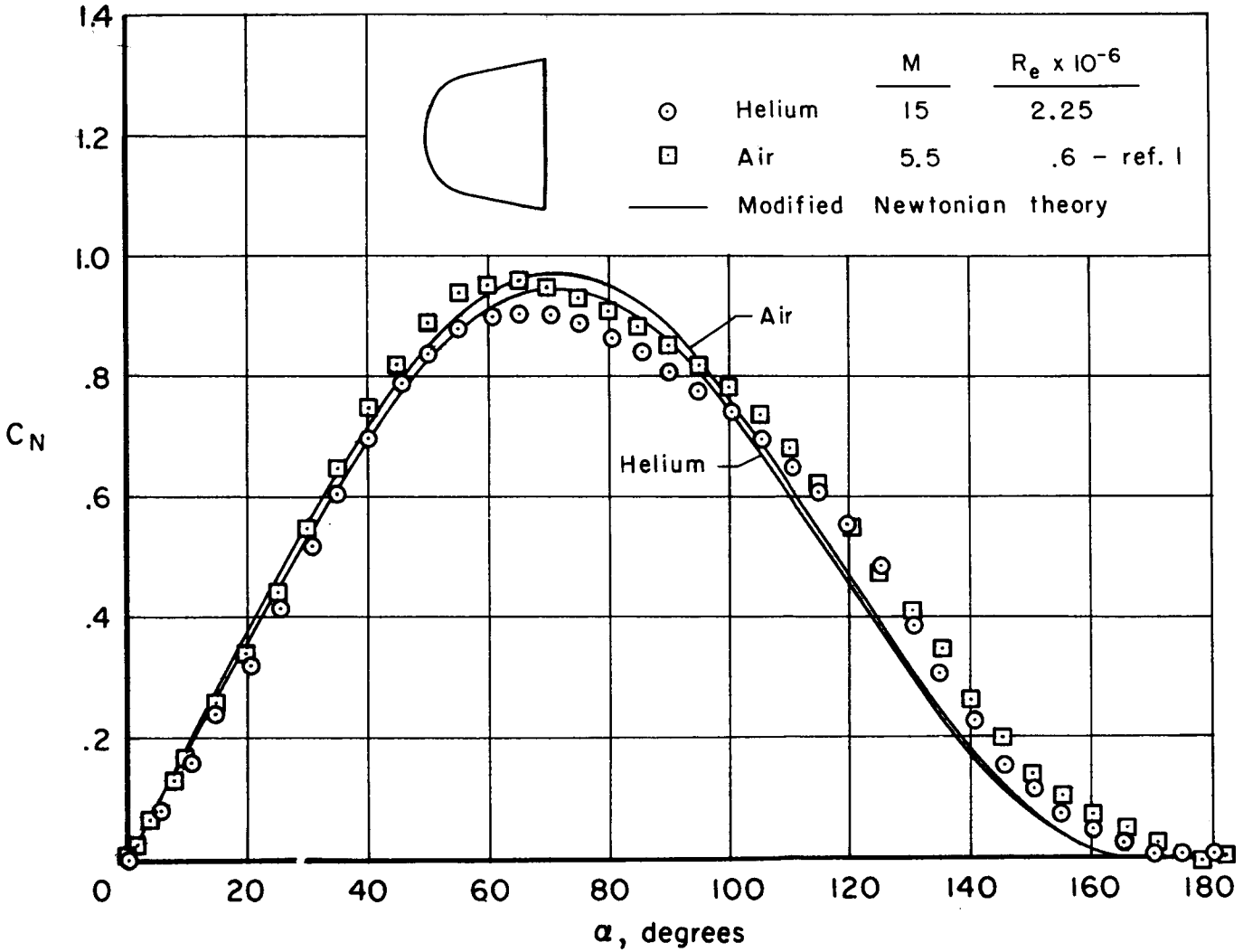

(b) C_N vs. α

Figure 6.- Continued.

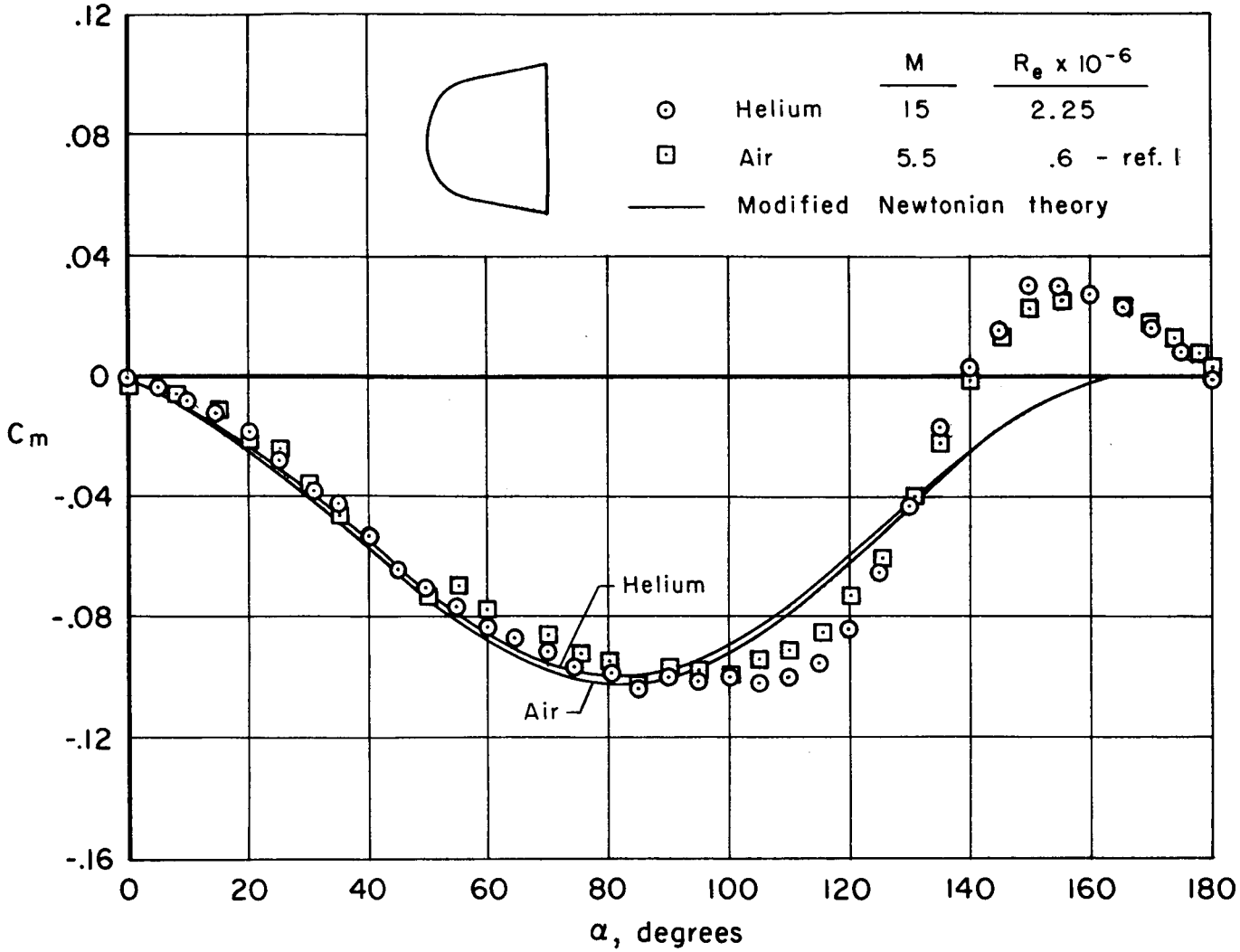

(c) C_m vs. α

Figure 6.- Concluded.

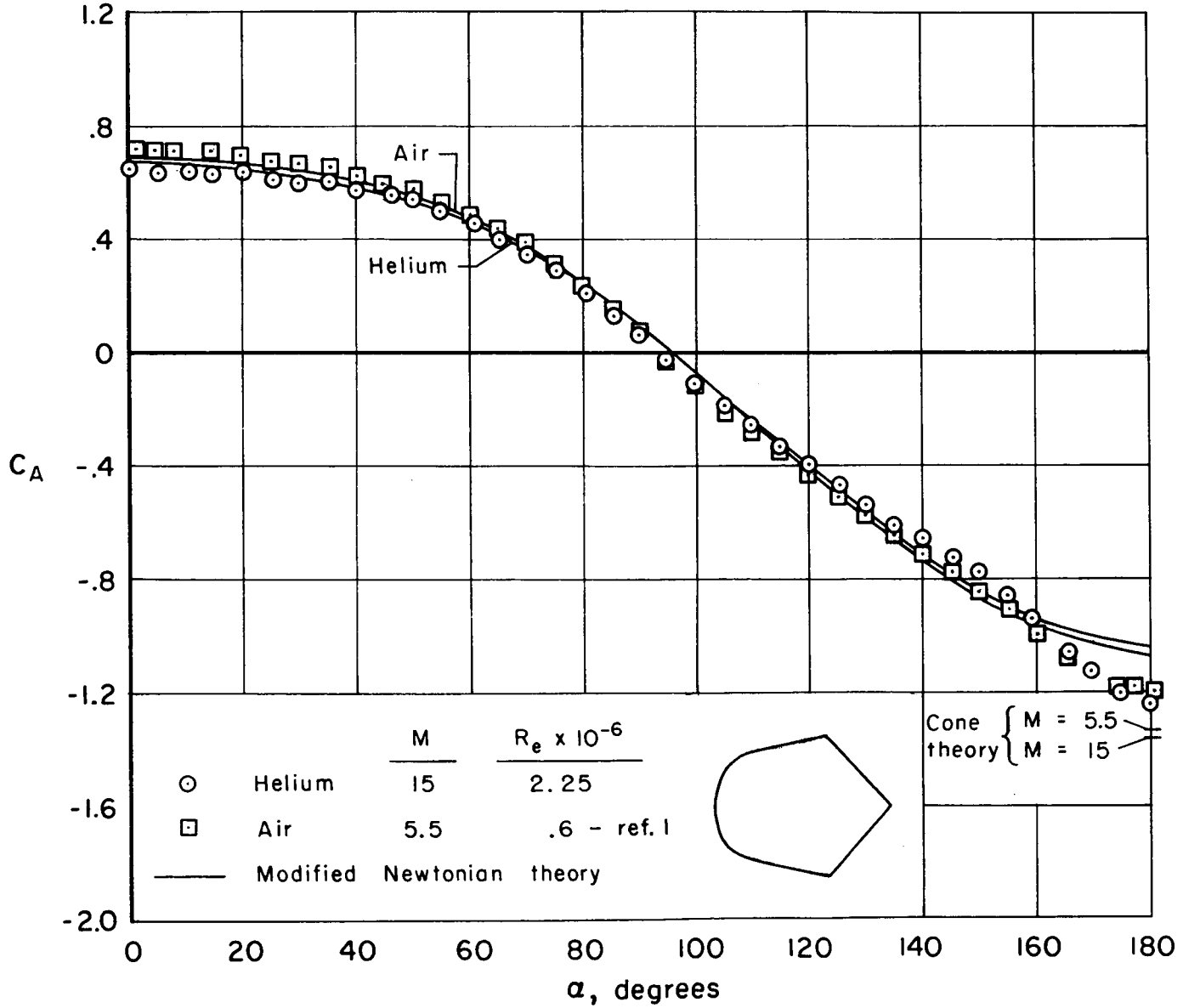

(a) C_A vs. α

Figure 7.- Comparison of static aerodynamic coefficients for model with afterbody obtained at M = 15 in helium and M = 5.5 in air.

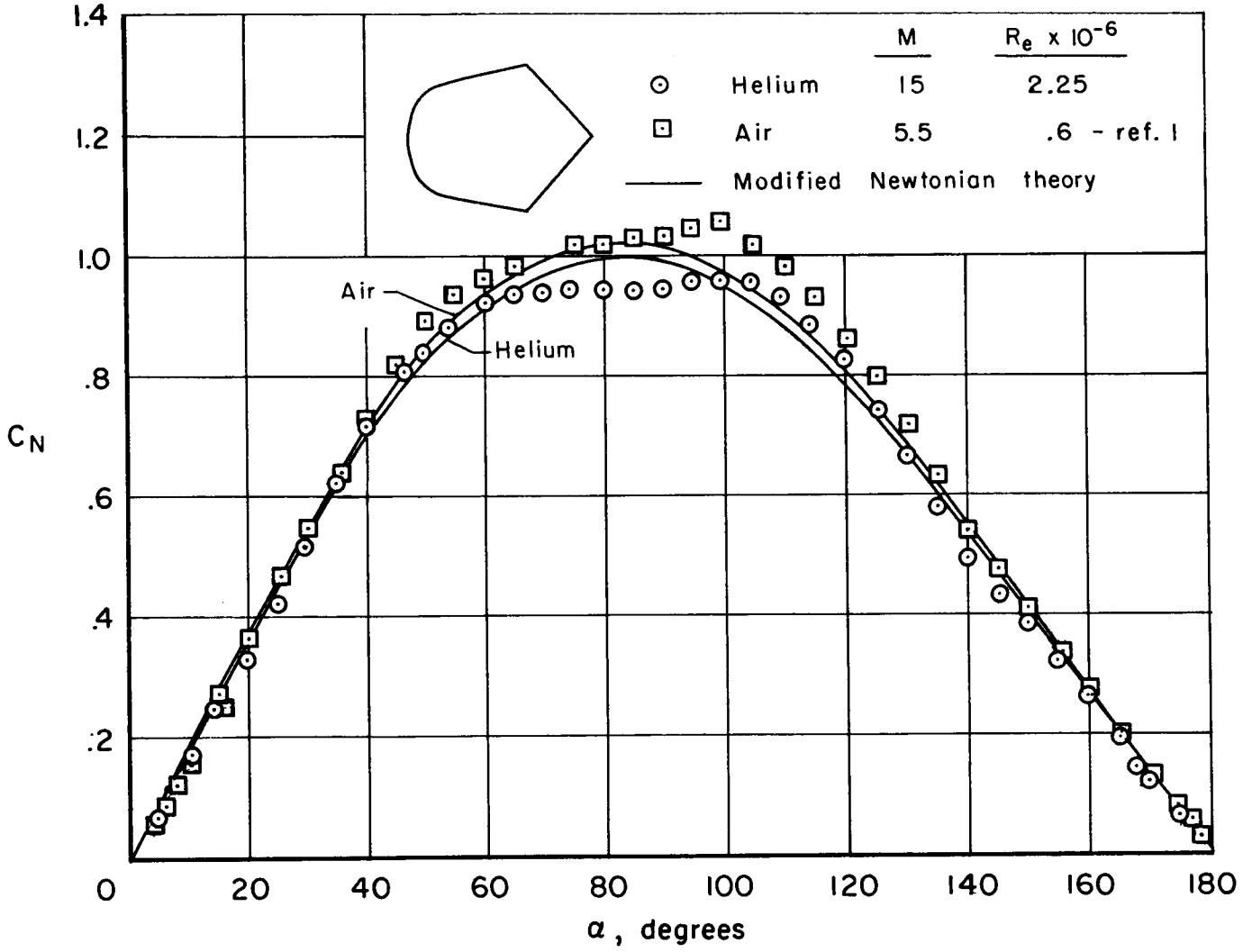

(b) C_N vs. α

Figure 7.- Continued.

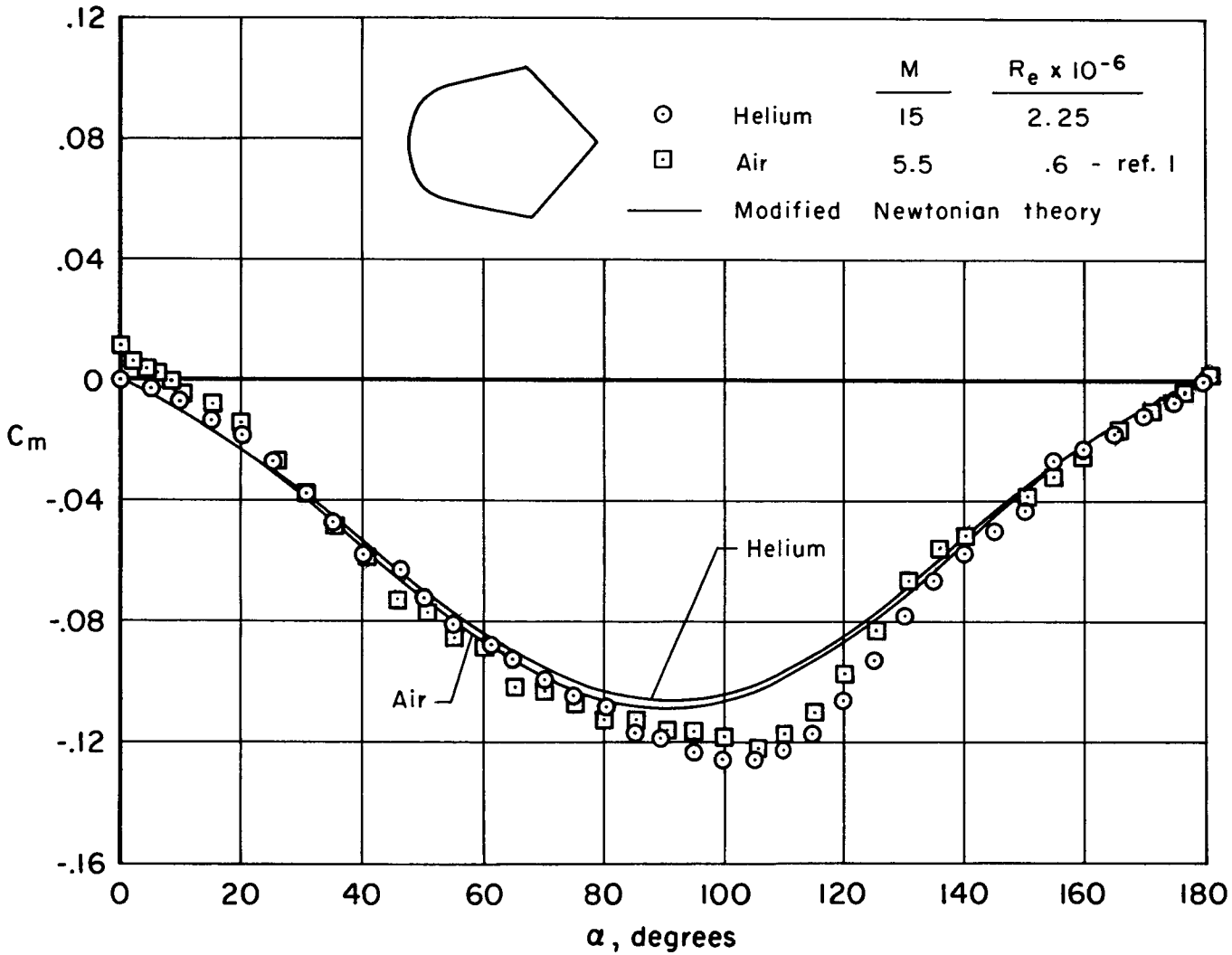

(c) C_m vs. α

Figure 7.- Concluded.

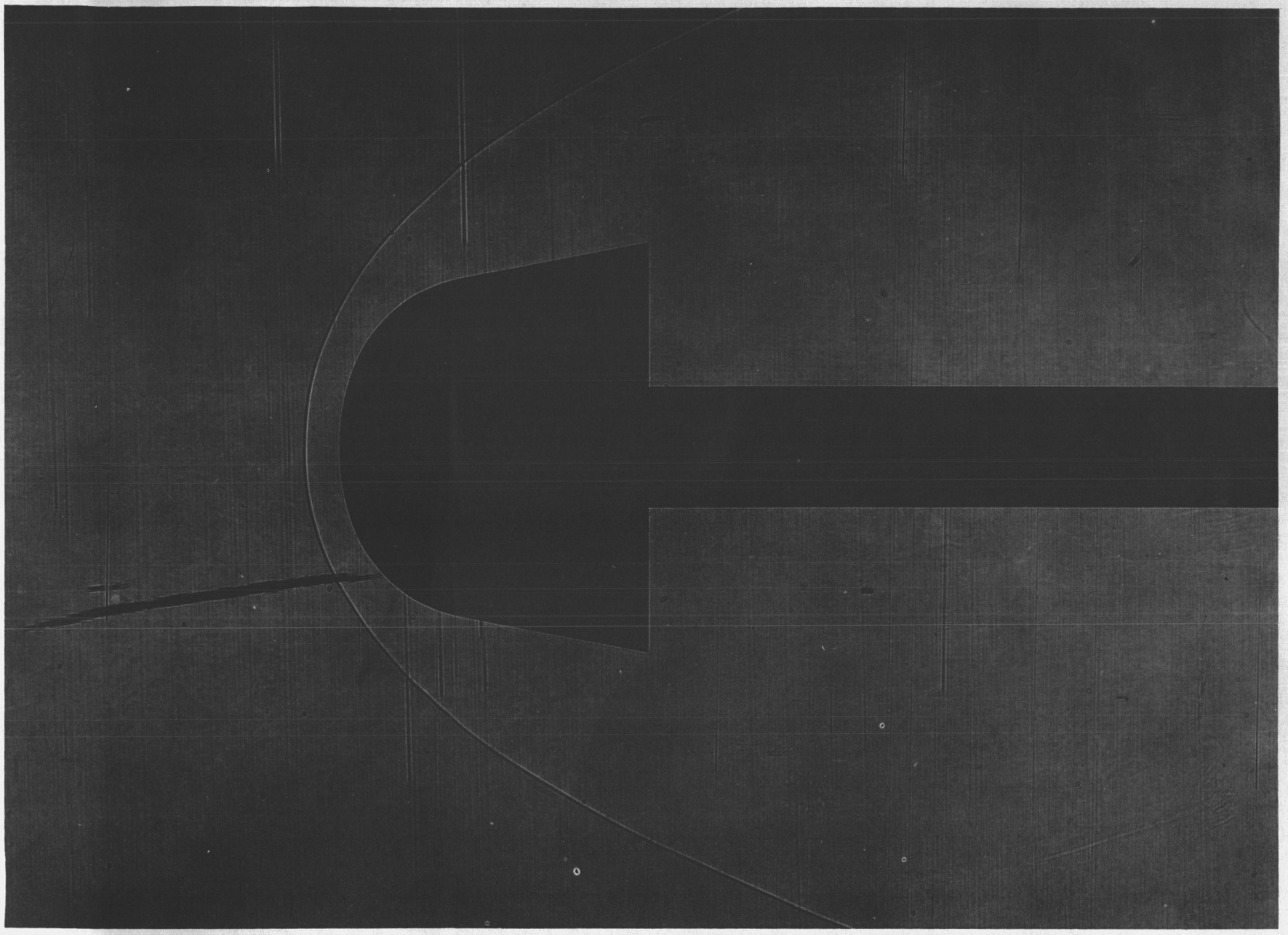

Figure 8.- Shadowgraph of model without afterbody in M = 15 helium flow, $\alpha = 0^{\circ}$.

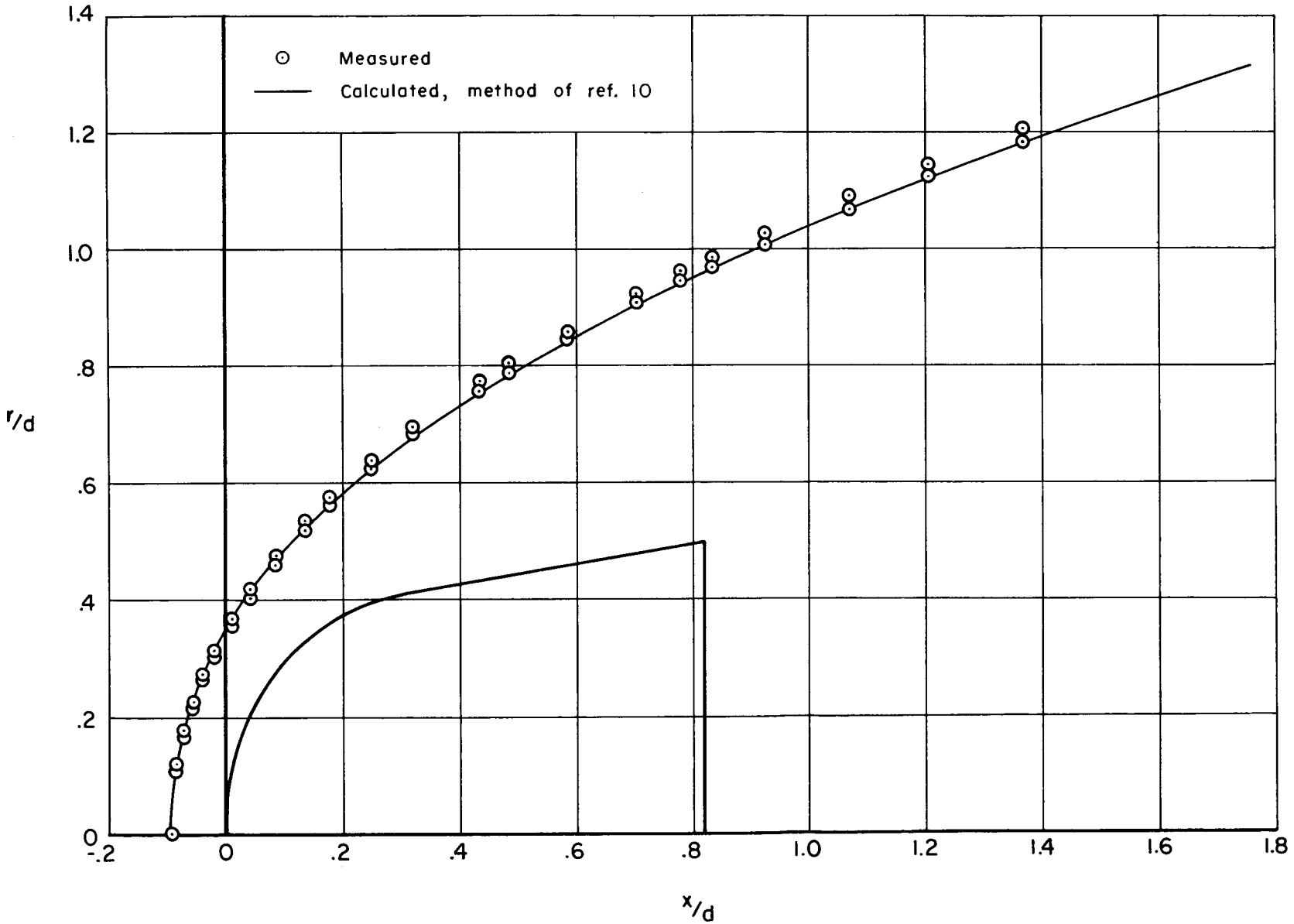

Figure 9.- Comparison of measured and predicted shock shapes for model without afterbody at M = 15 and $\alpha = 0^{\circ}$ in helium.

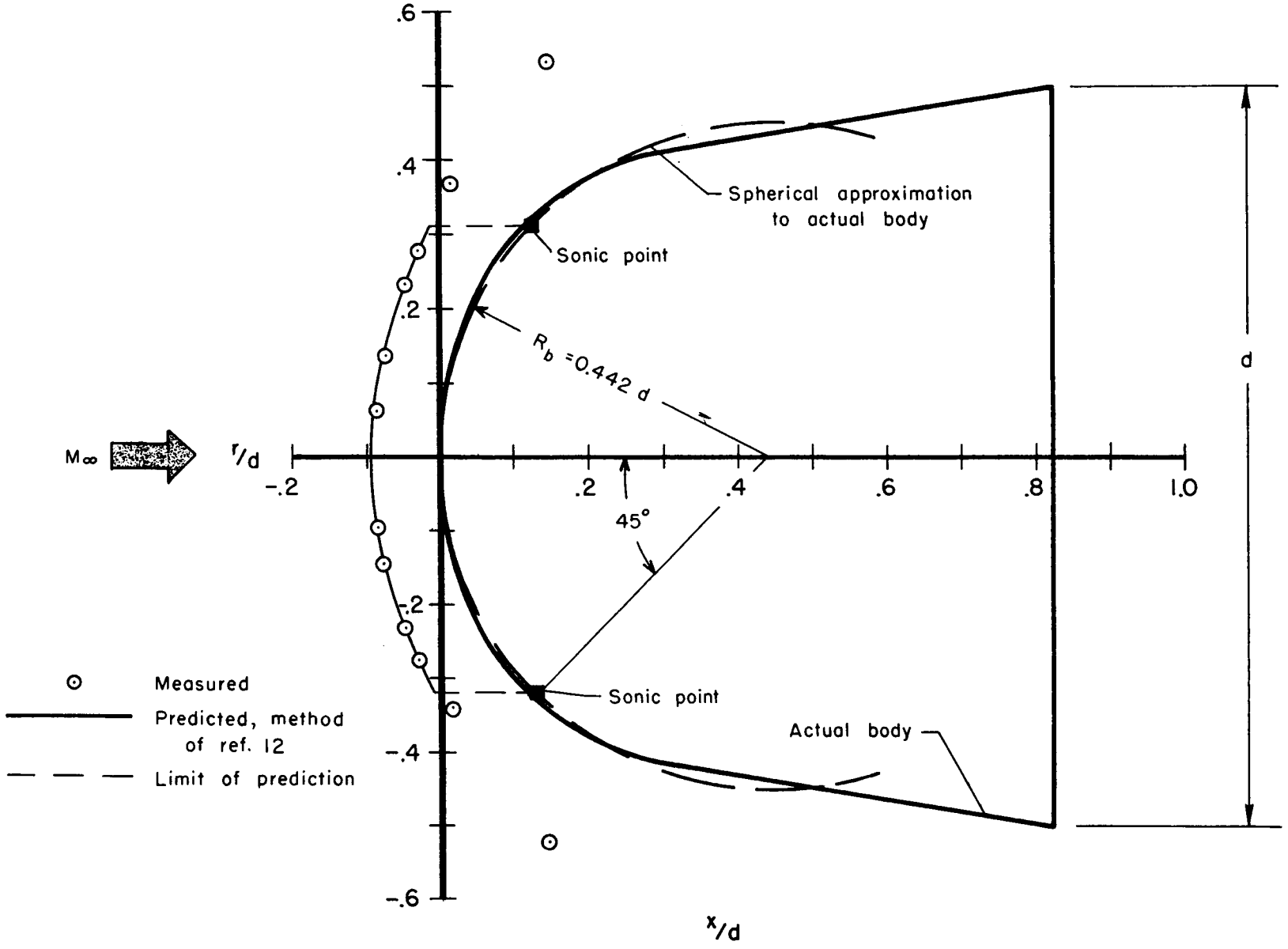

(a) $\alpha = 0^{\circ}$

Figure 10.- Comparison of measured and predicted shock shapes for model without afterbody at angle of attack and M = 15 in helium.

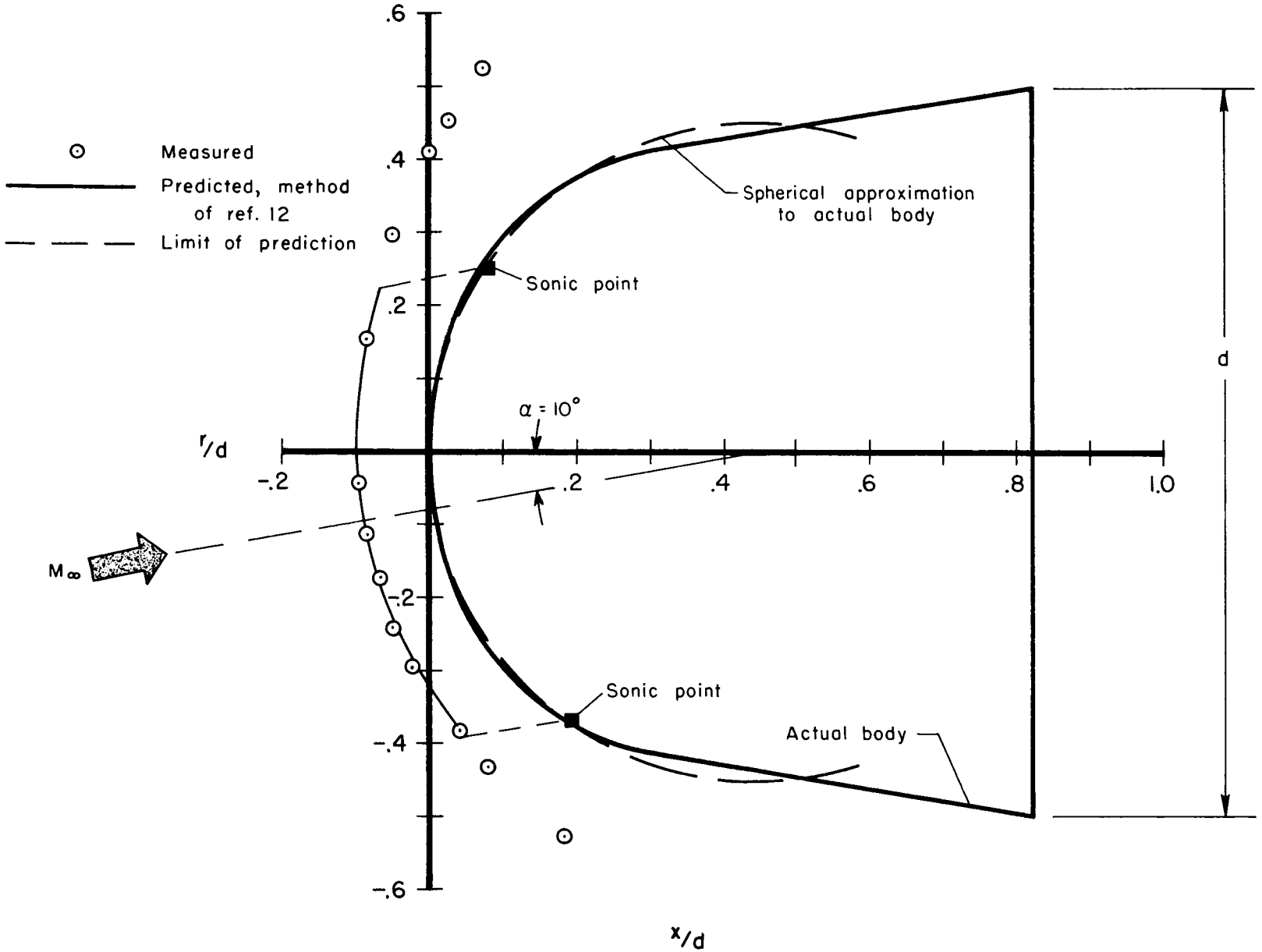

(b) $\alpha = 10^{\circ}$

Figure 10.- Continued.

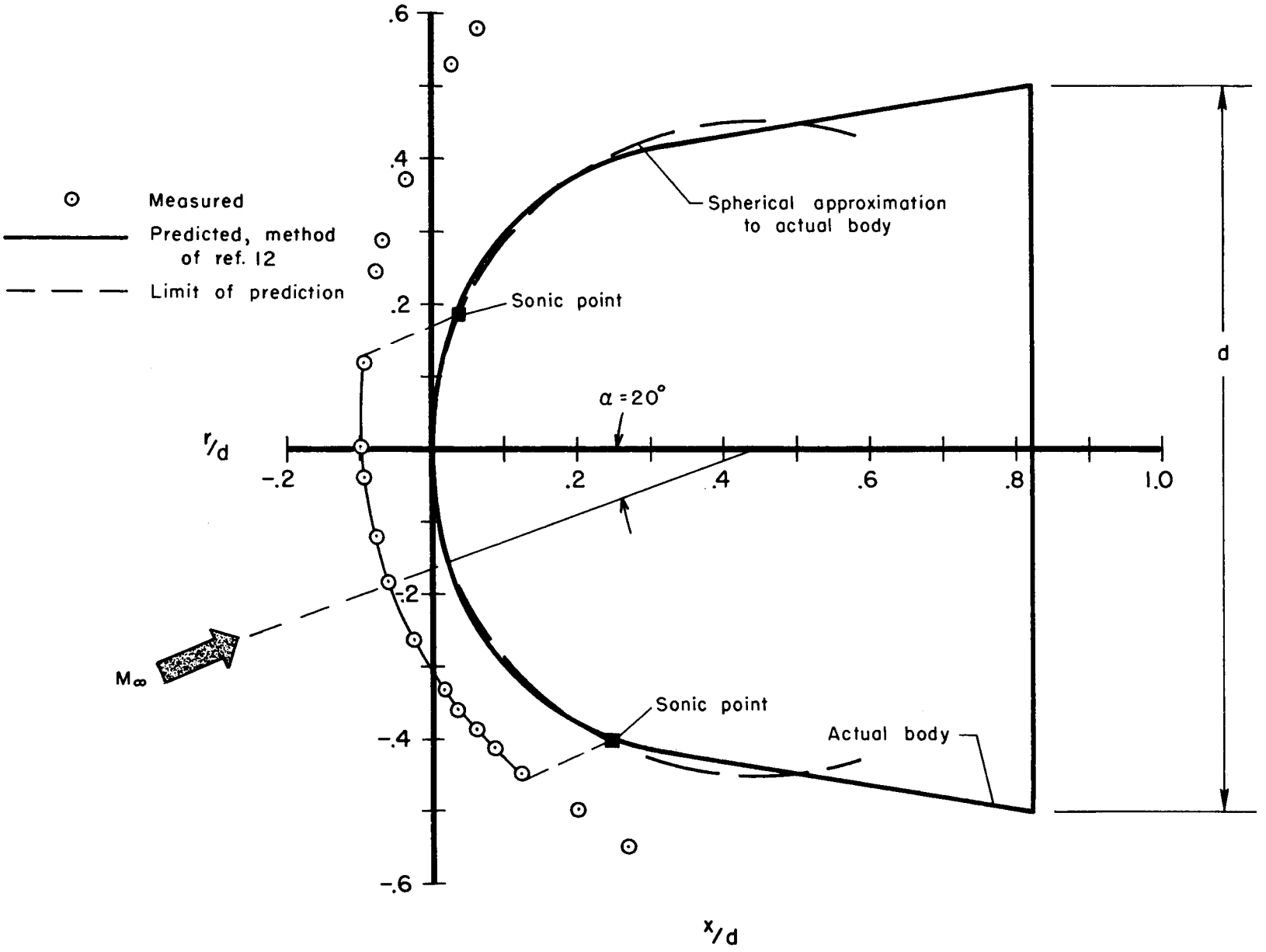

(c) $\alpha = 20^{\circ}$

Figure 10.- Continued.

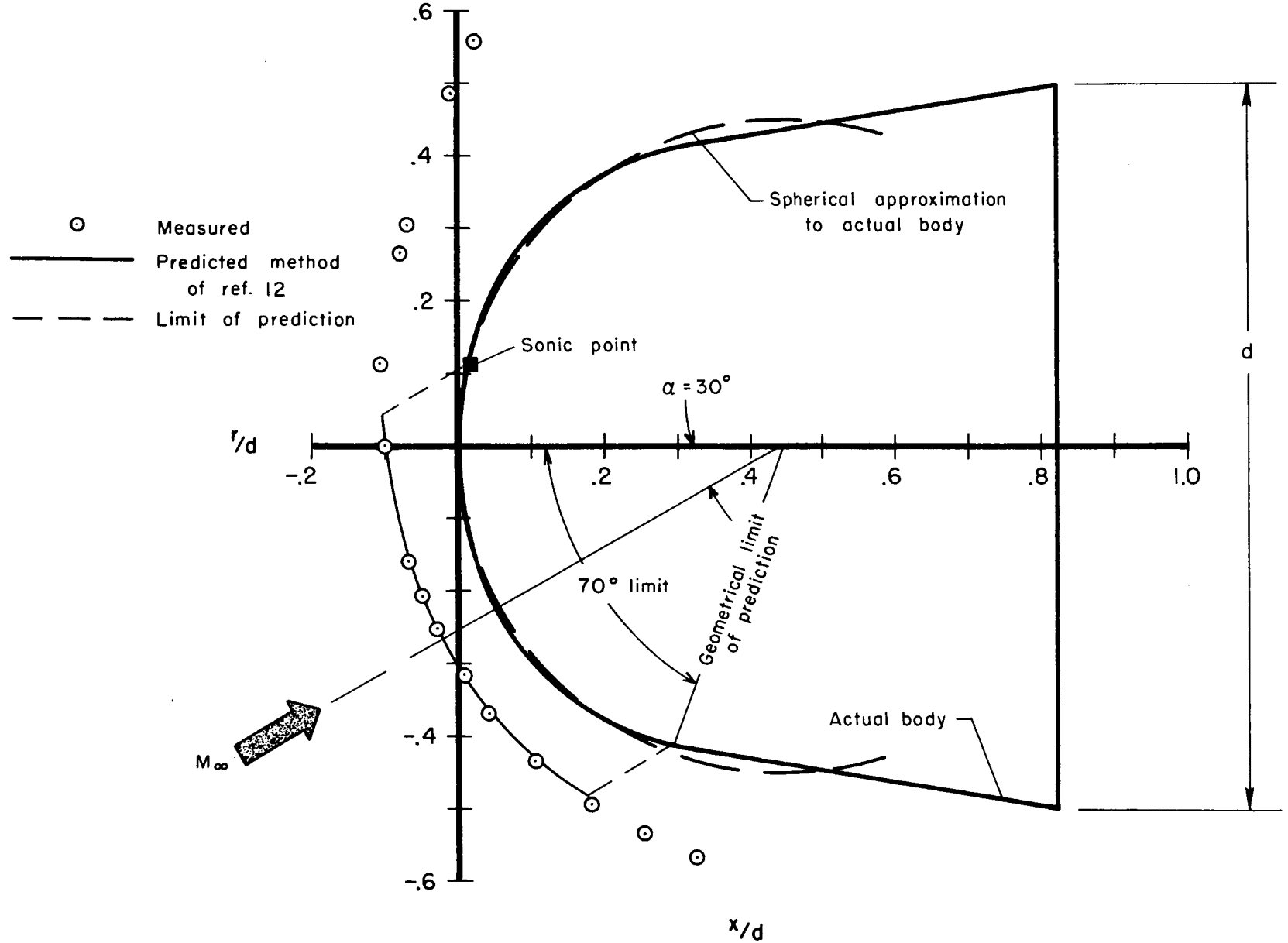

(d) $\alpha = 30^{\circ}$

Figure 10.- Continued.

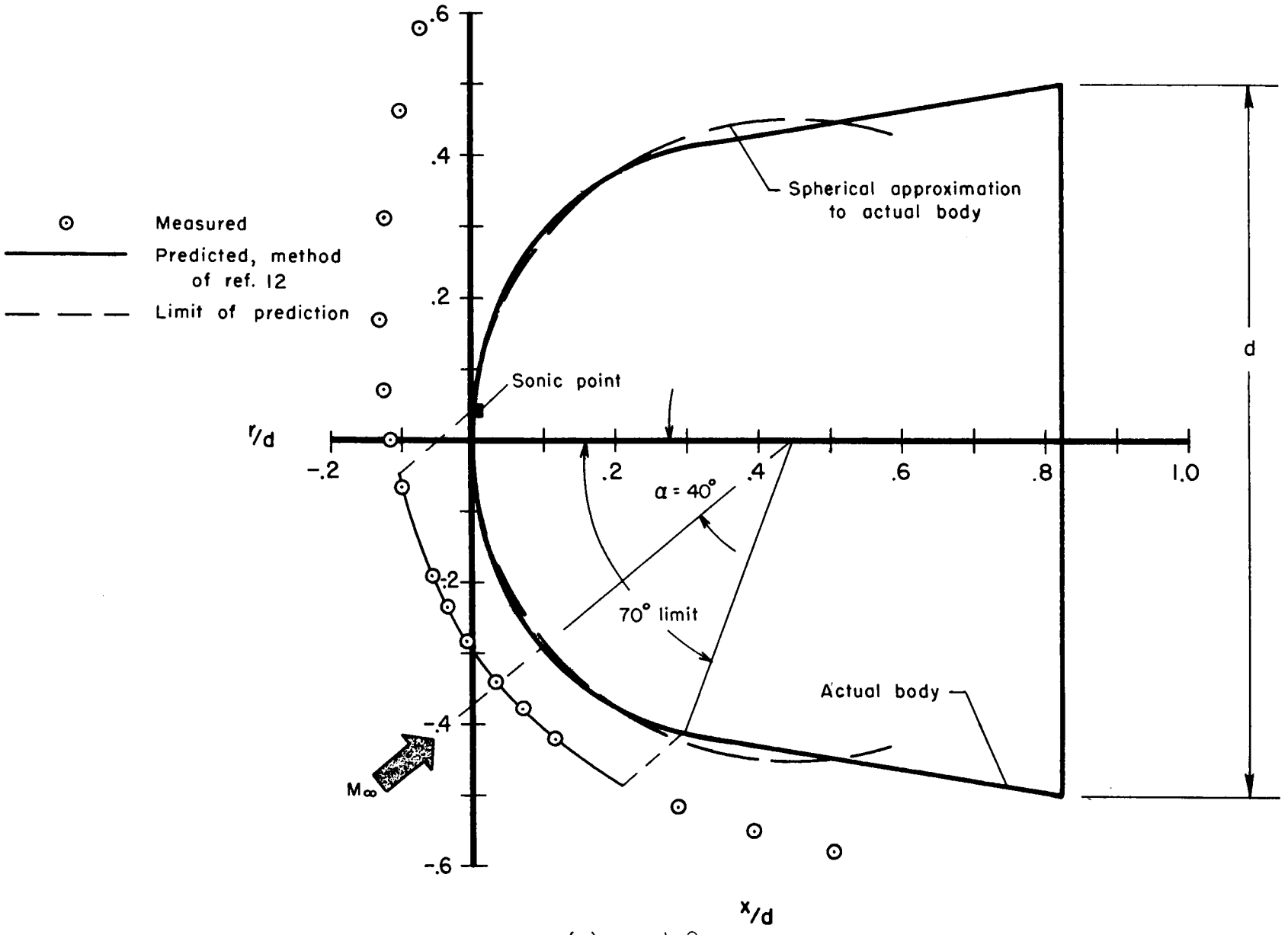

(e) $\alpha = 40^{\circ}$

Figure 10.- Continued.

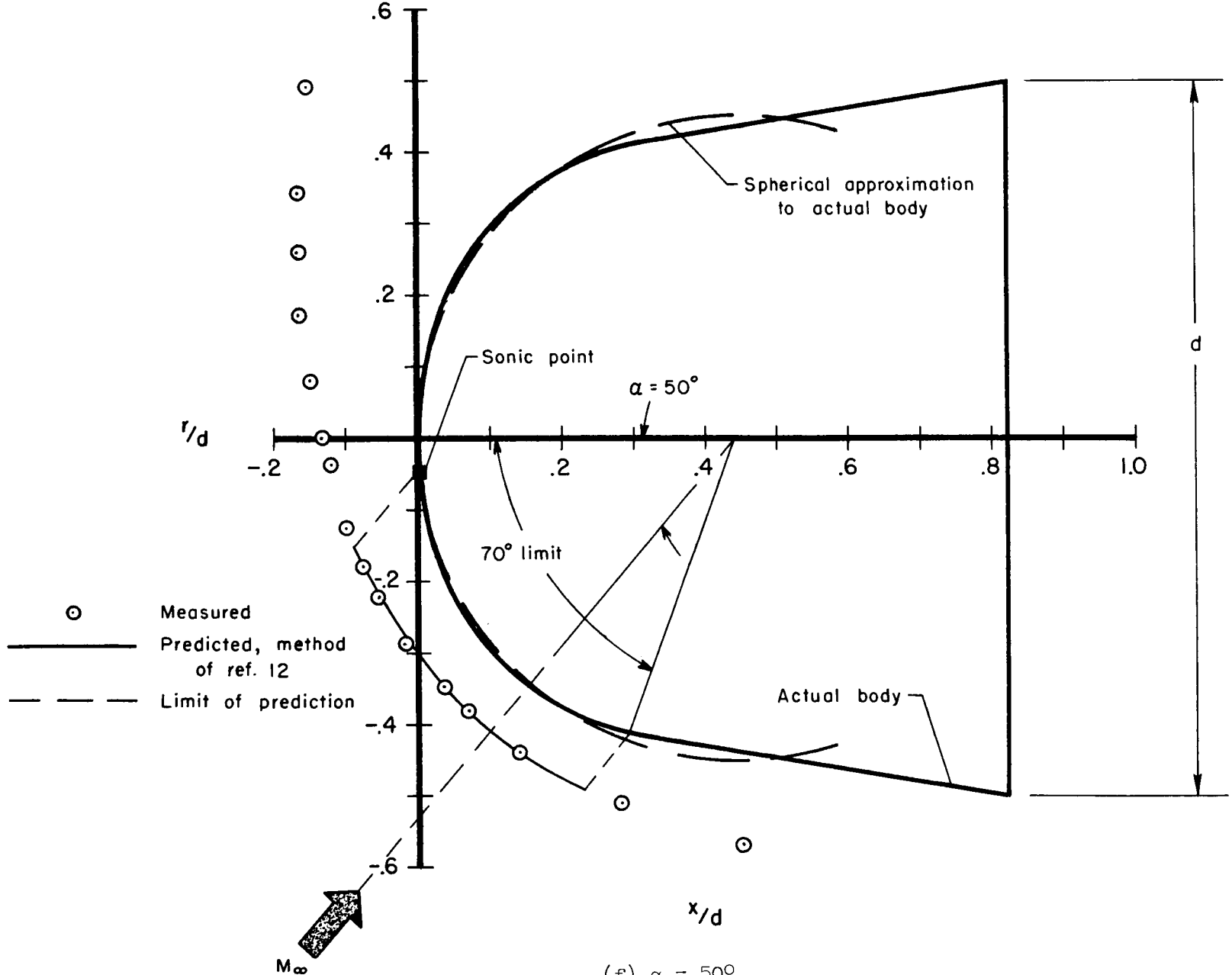

(f) $\alpha = 50^{\circ}$

Figure 10.- Continued.

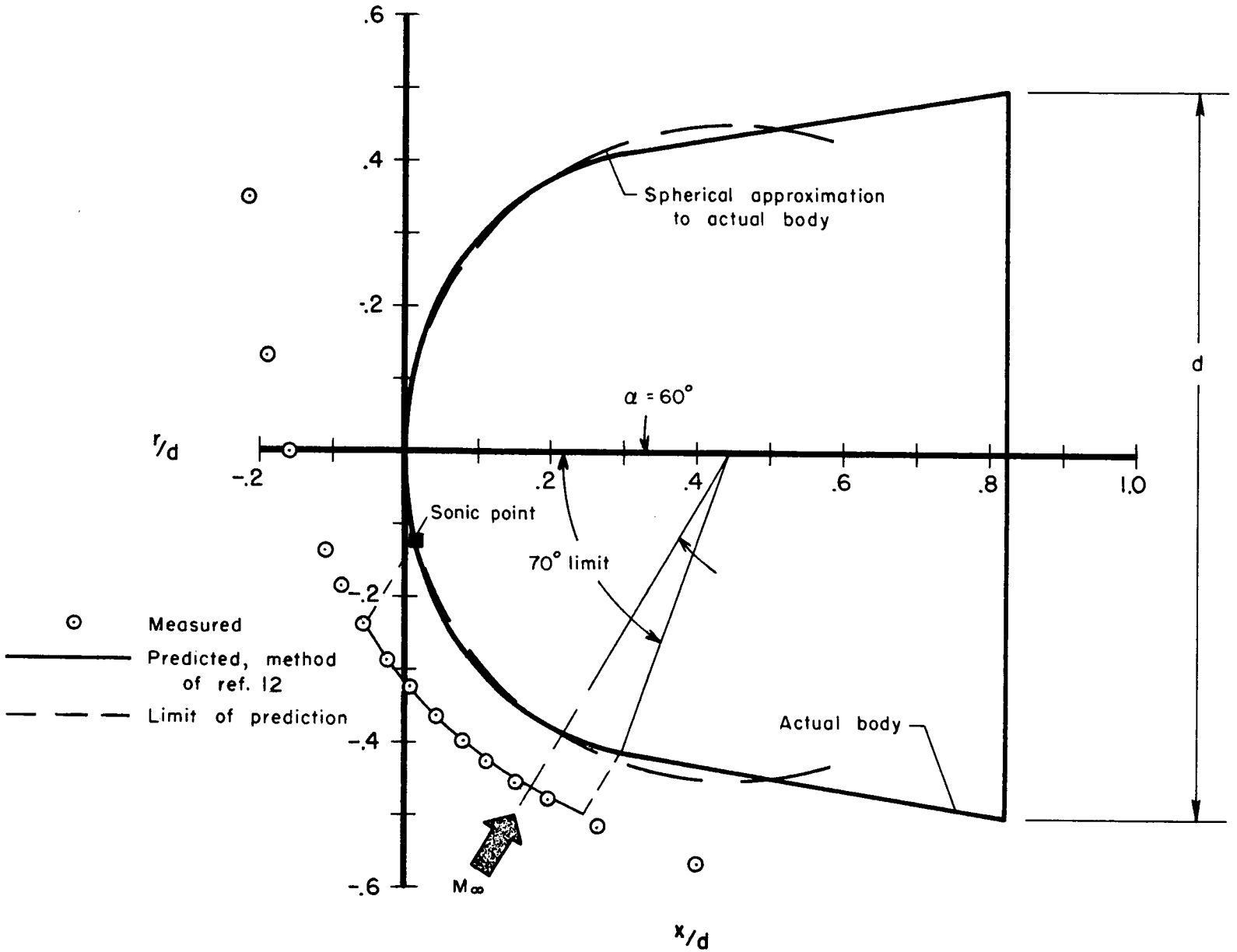

(g) $\alpha = 60^{\circ}$

Figure 10.- Continued.

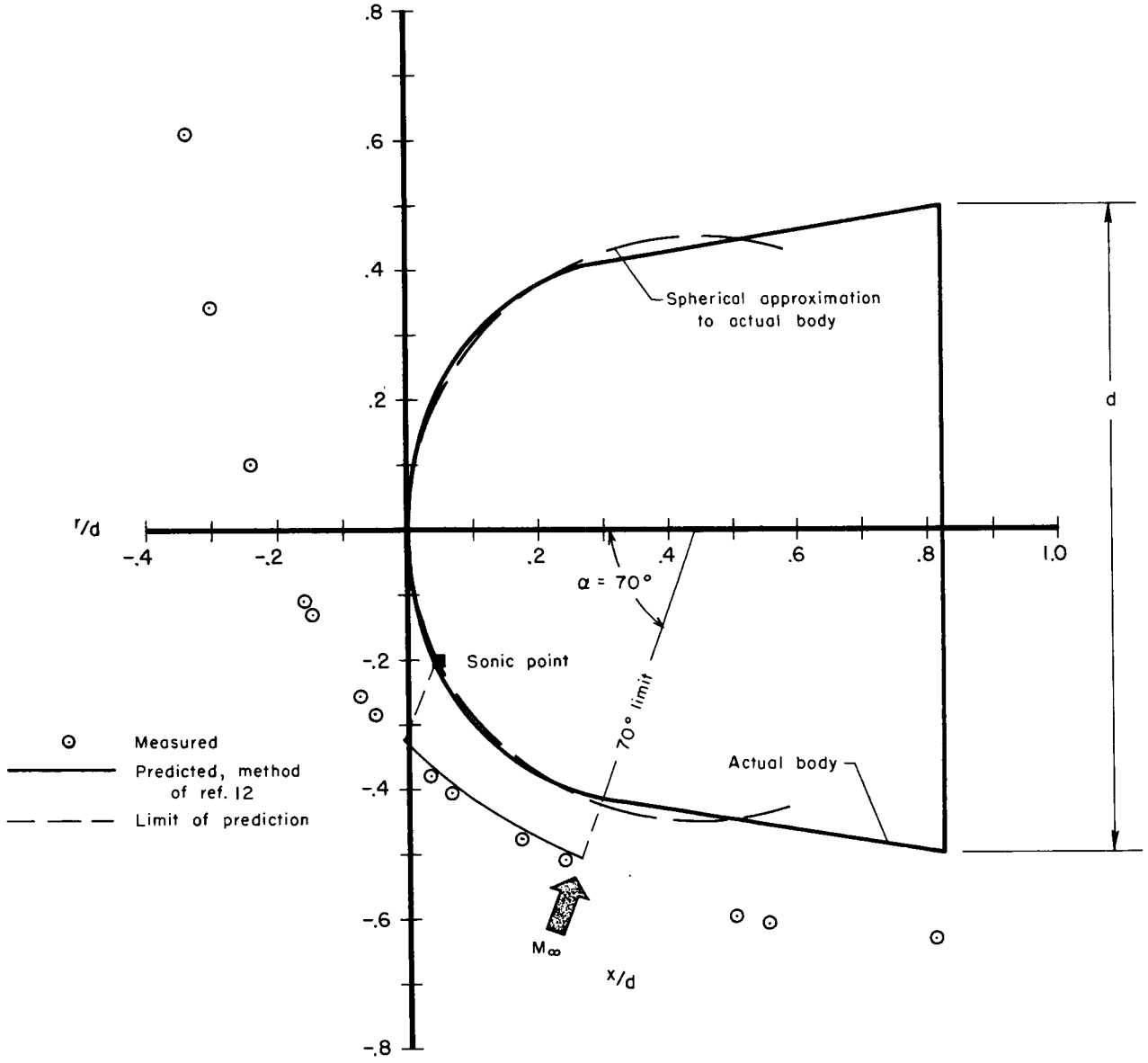

(h) $\alpha = 70^{\circ}$

Figure 10.- Continued.

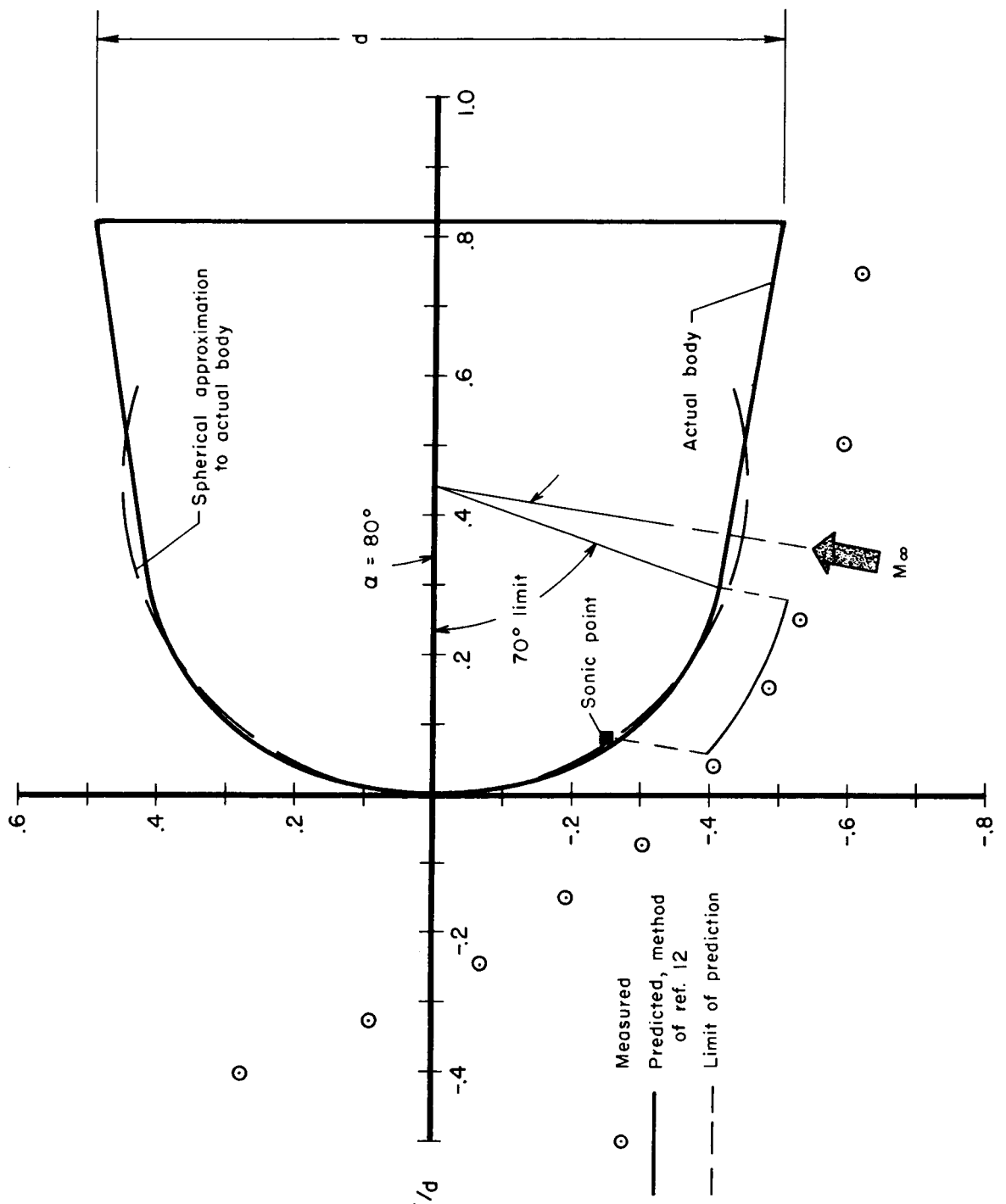

(i) $\alpha = 80^{\circ}$

Figure 10.- Concluded.